



## Temporal constraints and pulsed Late Cenozoic deformation during the structural disruption of the active Kashi foreland, northwest China

Richard V. Heermance,<sup>1,2</sup> Jie Chen,<sup>3</sup> Douglas W. Burbank,<sup>1</sup> and Jijung Miao<sup>4</sup>

Received 3 November 2007; revised 25 June 2008; accepted 17 July 2008; published 16 December 2008.

[1] In response to the ongoing Indo-Asian collision, structural deformation has encroached into the Tian Shan foreland in western China since the early Miocene. In order to reconstruct a detailed history of foreland deformation along the southern margin of the Tian Shan, we have synthesized extensive mapping, analysis of seismic sections, magnetostratigraphy of the foreland fill and associated growth strata, apatite fission track dating, changes in sediment accumulation rates, and geodetic surveys of deformed fluvial terraces. Across an area exceeding 6500 km<sup>2</sup> that spans the Kashi foreland in the northwestern Tarim Basin, we use these data to place temporal constraints on individual structures that delineate at least 4 distinct stages of deformation. Stage 1 involved initial uplift of hinterland structures beginning at 20–25 Ma. Stage 2 began at ~16.3 Ma when the basement-involved deformation front stepped south to the Kashi Basin Thrust that bounds the foredeep strata. Stage 3 occurred from 13.5 to 4 Ma, as the deformation front migrated south in episodic steps above thin-skinned detachment and ramp-flat folding. Finally, stage 4 began after 4 Ma with growth of the Keketamu Anticline followed by rapid southward migration of the deformation front to the Atushi and then Kashi detachment anticlines. On the basis of the deformed Tertiary strata and available seismic data, calculations of the minimum magnitude of shortening yield totals ranging from 10 to 32 km since the early Miocene, of which 7–12 km occurred since ~4 Ma. Although average shortening rates since 16.3 Ma were 0.8–1.3 mm/a, rates were faster from 16.3 to 13.5 Ma (1.1–3.2 mm/a), after which they decreased to 0.5 mm/a between 13.5 and 4 Ma before increasing to 2.2–2.7 mm/a after 4 Ma. Similarly, the rate of southward

propagation of the deformation front was initially 3–7 mm/a for the first 10 Ma of basin development, slowed to 1.5 mm/a between 13.5 and 4 Ma, and increased to more than 10 mm/a since 4 Ma. These changes in shortening and structural migration rates over time suggest that the loci of orogenic deformation shifted in and out of the foreland during the Neogene. Surveyed stream terraces suggest that, although most current deformation is located along the southern front of the foreland, modest deformation and shortening continue in the hinterland. Structural style within the foreland has also changed over time from imbricate thrust faults with hanging wall folds along the northern margin, to ramp-flat faults and detachment folds along the southern margin. Where the basement rocks are previously deformed, such as in the hinterland of the Kashi foreland, thick-skinned fault ramps and related fault propagation folds dominate the structural style. As syntectonic sedimentation within the foreland produced thick, subhorizontal stratigraphy, the structural style evolved to detachment and fault bend folding above these footwall flats within the Neogene strata. **Citation:** Heermance, R. V., J. Chen, D. W. Burbank, and J. Miao (2008), Temporal constraints and pulsed Late Cenozoic deformation during the structural disruption of the active Kashi foreland, northwest China, *Tectonics*, 27, TC6012, doi:10.1029/2007TC002226.

### 1. Introduction

[2] As collisional orogens grow, deformation encroaches upon and disrupts adjacent foreland basins. Traditional conceptual models of this foreland deformation argue that thrust faults step sequentially and unidirectionally forward across the foreland and that as each new fault is initiated, slip on the previously formed fault is abandoned [e.g., *Armstrong and Oriel*, 1965; *Dahlstrom*, 1970]. A contrasting perspective emerges from modern collisional ranges where seismicity commonly is distributed across the foreland [*Seeber et al.*, 1981] and out-of-sequence faulting is observed [*Kao and Chen*, 2000]. This perspective is reinforced by structural cross sections that require out-of-sequence (hinterland) thrusting to explain imbricate fault stacks [e.g., *Morley*, 1988; *Boyer*, 1992]; and by numerical and analog models of critically tapered wedges that require internal deformation within the wedge to maintain its taper

<sup>1</sup>Department of Earth Science, University of California, Santa Barbara, Santa Barbara, California, USA.

<sup>2</sup>Now at U.S. Geological Survey, Tucson, Arizona, USA.

<sup>3</sup>State Key Laboratory of Earthquake Dynamics, Institute of Geology, China Earthquake Administration, Beijing, China.

<sup>4</sup>Research Institute of Petroleum Exploration and Development, PetroChina, Beijing, China.

in the face of both erosion and accretion [Dahlen, 1990; Dahlen et al., 1984; Davis et al., 1983; Willett, 1999].

[3] In order to rigorously assess the applicability of these contrasting models to a given collisional range, the long-term slip history for multiple faults within the foreland fold-and-thrust belt needs to be known. Numerous studies have focused on the leading edge of active deformation in a collisional mountain belt [Delcaillau et al., 1998; Husson et al., 2003; Medwedeff, 1992; Mulder and Burbank, 1993], and for some ranges, almost all of the geodetic slip is occurring today within the forwardmost structures [Lavé and Avouac, 2000]. Despite many decades of study, however, only a relatively few forelands have yielded the sought after chronologies of sequential deformation [Burbank and Reynolds, 1984; Jordan et al., 1993; Meigs and Burbank, 1997]. The reasons for this paucity of data across forelands are that many chronologic studies have focused on only a single fold or fault [e.g., Charreau et al., 2006; Chen et al., 2002; Daeron et al., 2007; Delcaillau et al., 1998; Gonzalez-Mieres and Suppe, 2006; Simoes et al., 2007], growth strata are commonly not preserved for multiple faults within a foreland [Vergés et al., 2002], stratigraphic indicators of more hinterland deformation typically cannot be related to a specific fault [Najman et al., 2004], and many hanging walls have been buried to insufficient depths to cause resetting of thermochronologic indicators of deformation [e.g., Crowley et al., 2002; Sobel and Dumitru, 1997]. In the absence of studies that encompass all the major faults within a foreland, not only is it difficult to test whether faulting was sequential or out-of-sequence, but it is impossible to assess the steadiness of deformation: was fault propagation pulsed and episodic or uniform; was slip accumulation steady or were rates variable among different faults?

[4] In this study, we strive to address many of these questions by developing chronologies for multiple folds and faults and by calculating slip rates for each major structure across an actively deforming foreland. To accomplish this, we synthesized structural interpretations with magnetostratigraphy from more than 10 km of stratigraphic section at 11 localities [Heermance et al., 2007] in the deformed foreland along the SW margin of the Chinese Tian Shan, and combined these data with thermochronologically derived cooling histories for several basement-involved thrust faults [Sobel et al., 2006]. Within this new temporal framework, not only do we constrain the history of deformation across the Kashi foreland, but we show that accelerated rates of both shortening and basinward propagation of the deformation front in Plio-Pleistocene times coincided with the onset of major detachment folding within the foreland strata.

## 2. Geologic Setting

[5] The Neogene Kashi foreland basin, located between the north vergent Pamir and south vergent Tian Shan, forms the western corner of the Tarim Basin (Figure 1). The Kashi foreland contains >6 km of Tertiary strata [Allen et al., 1999; Bally et al., 1986; Heermance et al., 2007] derived from erosion of the adjacent orogen. Deformation over the last 25 Ma [Avouac et al., 1993; Sobel et al., 2006; Sobel

and Dumitru, 1997; Yin et al., 1998] has differentially exhumed the foreland deposits such that well-exposed stratigraphic sections are juxtaposed with Neogene structures across the arid foreland. Along the northern foreland margin, fault ramps place Paleozoic strata over Tertiary foreland sedimentary strata to the south. In contrast, deformation along the southern margin of the Kashi foreland is dominated by folding but not faulting (Figure 2). Active rivers cut these structures, providing an exceptional view of the three-dimensional foreland geometry and of the relationship between deposition and deformation [Chen et al., 2007]. The stratigraphic thickness within the Kashi foreland is 3–5 times greater than in the nearby Kepintage fold-and-thrust belt ~100 km to the east, where detachment folding is not present and deformation has penetrated over 30 km more into the Tarim Basin (Figure 1) [Yin et al., 1998].

[6] The Tian Shan is arguably the most spectacular example of active intracontinental deformation on Earth. The range stretches for ~2500 km east-west between 70 and 95°E longitude and 40–45°N latitude in central Asia and contains peaks exceeding 7000 m in elevation. The Tarim Basin flanks the southern edge of the Tian Shan where it forms an internally drained basin that captures sediments eroded from the actively uplifting range. Foreland sediments within the Tarim Basin provide a sedimentary record of uplift and erosion in central Asia from the Paleozoic to present [Carroll et al., 1995; Charreau et al., 2005, 2006; Hendrix et al., 1992; Huang et al., 2006; Ji et al., 2008; Métivier and Gaudemer, 1997; Sun et al., 2004]. In addition, deformation of Cenozoic foreland sediments provides a record of recent growth of the Tian Shan [Allen et al., 1999; Chen et al., 2007; Daeron et al., 2007; Gonzalez-Mieres and Suppe, 2006; Yin et al., 1998].

[7] The tectonic history of central Asia during the Phanerozoic spans at least 400 million years. Major collisional events occurred during the Late Devonian to Early Carboniferous and Late Carboniferous to Early Permian, resulting in the complete amalgamation of the Tian Shan region of the Asian continent [Carroll et al., 1995; Dumitru et al., 2001; Windley et al., 1990]. At least three deformational events occurred in the Mesozoic as a result of the accretion of continental blocks to the South Asian margin [Hendrix et al., 1992]. From the late Cretaceous to the Oligocene, tectonic quiescence within the western Tian Shan produced an erosion surface marked by a sharp unconformity [Abdrakhmatov et al., 2001; Allen et al., 1991], and this erosional unconformity provides a distinctive marker horizon within the Kashi area [Heermance et al., 2007].

[8] Tertiary uplift of the Tian Shan was a delayed response to the continental collision between India and Eurasia [Molnar and Tapponnier, 1975]. Moreover, the timing of uplift varies from east to west and north to south within the range. In a general sense, uplift commenced along the southern margin between 20 and 25 Ma on the basis of apatite fission track cooling history [Hendrix et al., 1994; Sobel et al., 2006; Sobel and Dumitru, 1997]. Increased sedimentation rates and thermochronology along the northern Tian Shan range front imply that rock uplift did not initiate until ~11 Ma in both the Kyrgyz [Bullen et al.,

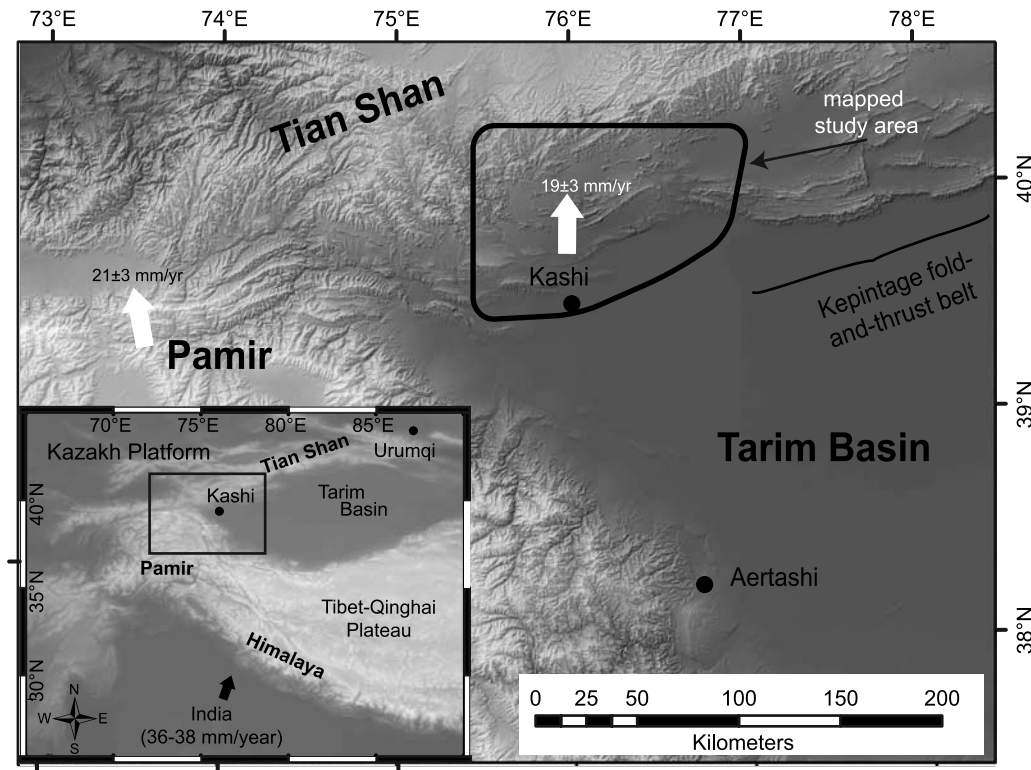


**Figure 1.** Shaded relief digital elevation model of the southwestern Chinese Tian Shan. Arrows indicate global positioning system shortening rates relative to the stable Kazakh platform [Reigber *et al.*, 2001; Wang *et al.*, 2001]. Notice how the Kepintage fold-and-thrust belt has penetrated further into the Tarim Basin than the adjacent Kashi foreland.

2001, 2003] and Chinese [Charreau *et al.*, 2005] Tian Shan, although Ji *et al.* [2008] infer uplift at  $\sim 26$ – $22$  Ma as well as  $\sim 11$  Ma on the basis of increased sedimentation rates. These different initial uplift ages imply that deformation has progressed asymmetrically across the range and may have slowly migrated northward during the Miocene. A regional increase in sedimentation and exhumation is observed circa 3–4 Ma on many margins of the Tian Shan [Bullen *et al.*, 2001, 2003; Heermance *et al.*, 2007; Métivier and Gaudemer, 1997; Sun *et al.*, 2004], and may be the result of either an increase in shortening or a change in climate and erosional unloading in the region [Burchfiel *et al.*, 1999; Molnar, 2004]. Within the northern Tarim Basin, other local deformation events have been inferred at 16–15 Ma and 7 Ma on the basis of sedimentation rate changes within the Kuqa Basin [Huang *et al.*, 2006].

[9] Total shortening is difficult to constrain across the Tian Shan because of a lack of key geologic data that span the entire range. Avouac *et al.* [1993] nevertheless estimated shortening of  $125 \pm 30$  km at  $87^\circ$  longitude to  $200 \pm 50$  km at  $76^\circ$  longitude, on the basis of Airy isostatic compensation of assumed crustal thickening. Along the southern foreland, minimum shortening is estimated at  $\sim 20$ – $40$  km along most of the range (from  $\sim 75$ – $85^\circ$ ), but decreases to  $\sim 10$ -km shortening at  $87^\circ$  near the eastern termination of the mountain belt [Allen *et al.*, 1999; Burchfiel *et al.*, 1999;

Sobel and Dumitru, 1997; Yin *et al.*, 1998]. Calculated shortening rates along the range front vary from 1 to 2 mm/a on the basis of initiation of uplift at 20–24 Ma [Allen *et al.*, 1999; Yin *et al.*, 1998] to 14 mm/a on the basis of most deformation having occurred since 2.5 Ma [Burchfiel *et al.*, 1999]. This latter estimate is based on deformation of the Xiyu Conglomerate with an assumed age of  $< 2.5$  Ma. The Xiyu Conglomerate, however, is time-transgressive at range and basin scale [Charreau *et al.*, 2005; Heermance *et al.*, 2007] and varies in age from 15.5 Ma to Quaternary. Hence, without knowledge of the local age of marker horizons, such as the Xiyu Conglomerate, reliable long-term rates are difficult to obtain. Active shortening along the modern Tian Shan in China occurs primarily on the southernmost structures on the basis of geomorphic surfaces [Daeron *et al.*, 2007; Schärer *et al.*, 2006], fault and fold scarps [Hubert-Ferrari *et al.*, 2005], and seismic activity [Allen *et al.*, 1999].

[10] Global positioning system (GPS) data collected over the past 15 years provide present-day shortening rates throughout central Asia to compare with geologically determined rates. Shortening between the Tarim plate and stable Eurasia reach a maximum of  $\sim 20$  mm/a [Abdrakhmatov *et al.*, 1996; Reigber *et al.*, 2001; Wang *et al.*, 2001] between  $73$  and  $77^\circ$  longitude (Figure 1). East along the range front, geodetic shortening rates decrease to less than 10 mm/a at  $84^\circ$  longitude [Reigber *et al.*, 2001] and then to less than

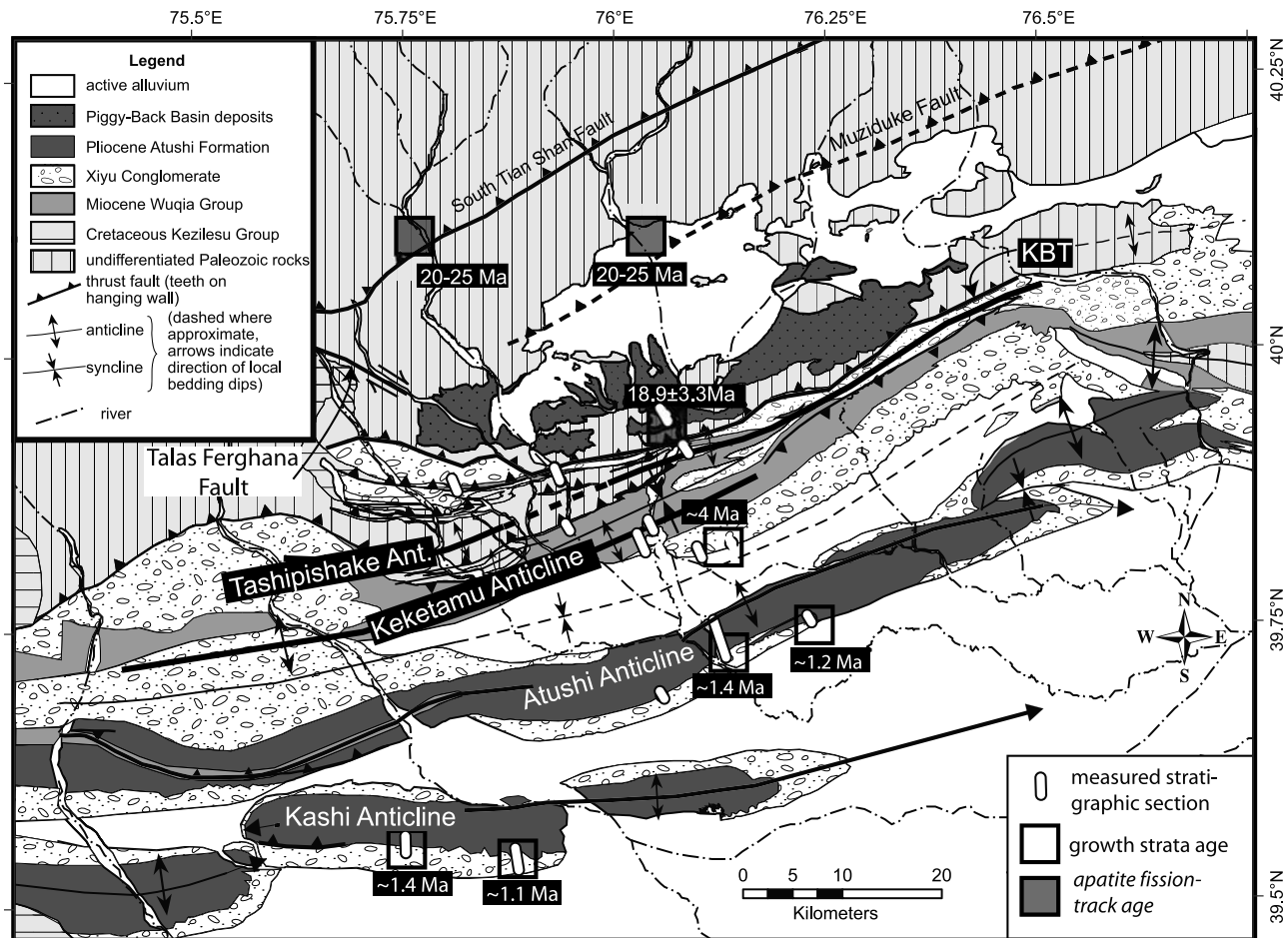


**Figure 2.** Geologic map of the study area. Boxed areas are locations where the initiation of uplift and deformation is interpreted on the basis of either growth strata [Chen *et al.*, 2007; Heermance *et al.*, 2007] or apatite fission track cooling data [Sobel *et al.*, 2006].

1 mm/a by 87° longitude [Wang *et al.*, 2001]. This more than twofold eastward decrease in geodetic rates over 1500 km has been attributed to rotation of the Tarim plate with respect to Eurasia about an Euler pole at 94°E, 37°N [Reigber *et al.*, 2001; Thatcher, 2007] or 96°E, 43.5°N [Avouac *et al.*, 1993] in the eastern Tarim Basin.

### 3. Kashi Foreland Stratigraphy

[11] The Kashi foreland basin in northwest China contains more than six kilometers of Neogene and Quaternary sediments that unconformably overlie Paleozoic and/or Cretaceous bedrock (Figure 3) [Bally *et al.*, 1986; Heermance *et al.*, 2007]. These strata provide a record of syntectonic deposition within the tectonically subsiding basin since initiation of range uplift, and they provide marker horizons to constrain shortening across the basin. Detailed stratigraphic description and magnetostratigraphy from Heermance *et al.* [2007] is combined with new geologic mapping and structural interpretations to infer the basin geometry, shortening and timing of tectonic events.

[12] The Neogene strata within the Kashi foreland consist of fluvial and lacustrine sedimentary rocks that generally coarsen up-section. Middle Miocene, gypsiferous, lacustrine strata unconformably overlie Paleozoic, Cretaceous, and Lower Tertiary sedimentary units at the base. The Xiyu Conglomerate caps most sections of the basin. Being both thicker and stratigraphically lower in the north than in the south, and the Xiyu defines a wedge that thins and inter-fingers with the more distal, finer-grained sediments along the southern deformation front (Figure 3a). Overall, we have divided foreland strata into nine units on the basis of stratigraphic position, lithofacies and previous nomenclature (Figure 3a) [Heermance *et al.*, 2007]: Paleozoic, Cretaceous, Lower Tertiary, Wuqia group units A, B, C, and Pakabulake, Atushi, Xiyu, and Piggyback Basin. In the midst of our study area, the total measured thickness of the foreland strata is 6000 m, but thickens toward the west to as much as 9 km thick [Bally *et al.*, 1986]. Kashi foreland strata are briefly described here from oldest to youngest.

[13] Paleozoic rocks comprise Permo-Carboniferous marine strata that constitute the upper part of the Tarim platform.

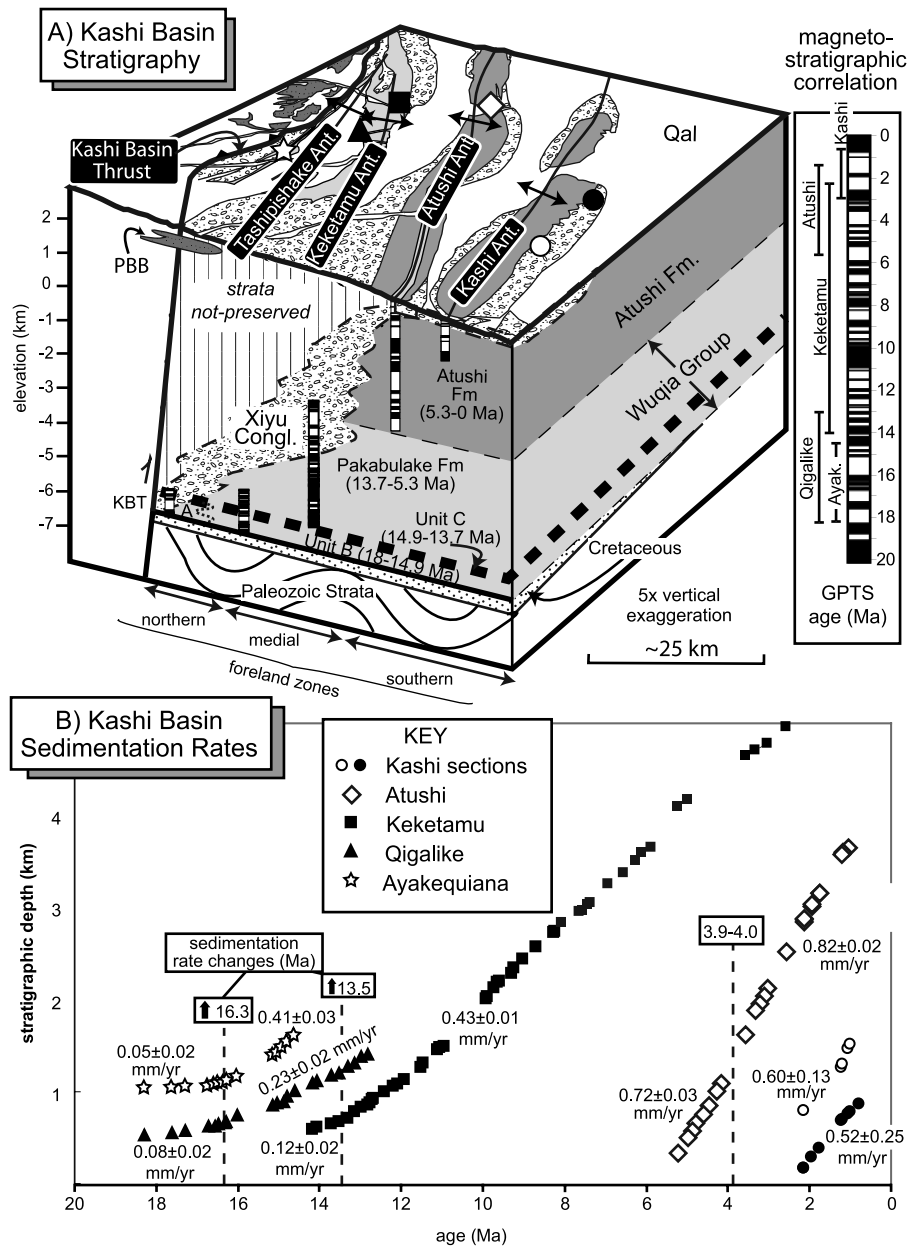


**Figure 3.** Plots of stratigraphy and sedimentation rates within the Kashi foreland. (a) Schematic geometry of the Kashi Basin based on surface mapping (top) and magnetostratigraphic sections from *Heermance et al.* [2007]. Stratigraphic sections are correlated along the basal unconformity and by bed tracing between sections. Ages of the formations are from the magnetostratigraphy correlated with the geomagnetic polarity timescale (GPTS) of *Lourens et al.* [2005] at the right. (b) Plot of stratal age versus stratigraphic depth for all the magnetostratigraphic sections [*Heermance et al.*, 2007]. Breaks in slope represent changes in sedimentation rate. Errors on the calculated sedimentation rates are 2-sigma least square regression errors. Boxed numbers (e.g., 13.5) indicate the age of the observed sedimentation rate changes.

At least 5 km of Paleozoic strata are exposed east of the study area in the Kepintage thrust belt [*Allen et al.*, 1999; *Carroll et al.*, 1995; *Yin et al.*, 1998], where they are exposed below a subparallel disconformity with the overlying Tertiary rocks (Figure 4a). These same Paleozoic strata, however, are intensely deformed below an abrupt

angular unconformity in the Kashi Region (Figures 4b and 4c), suggesting pre-Tertiary deformation in this area. In general, the Paleozoic stratigraphy consists of fossiliferous dark gray Carboniferous carbonates overlain by ~50 m of dark red marine shale and capped by more than 500 m of well-bedded, tan and gray fluvial sandstone and shale.

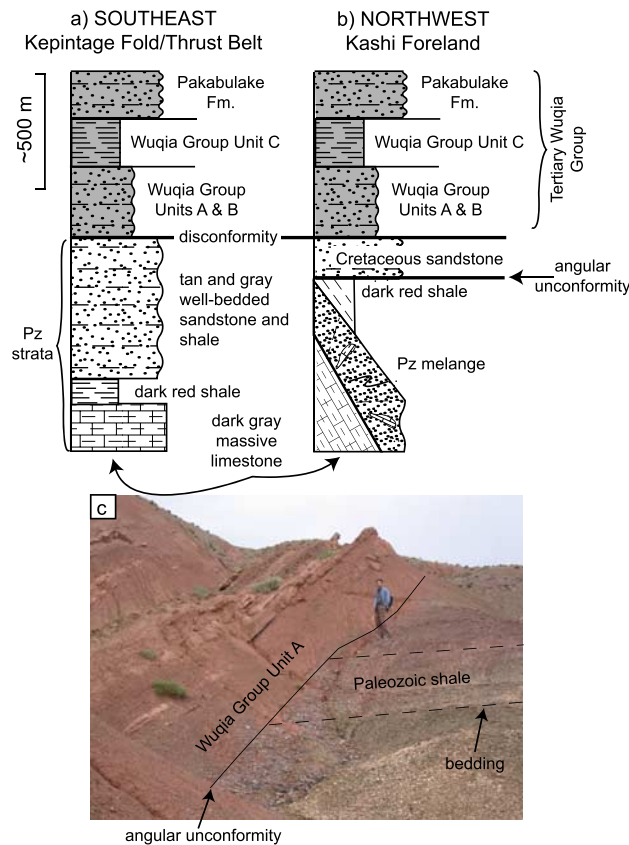


**Figure 4.** Schematic stratigraphic sections to show the relationship between the Paleozoic structure in the southeastern (a) and northwestern (b) part of the Kashi foreland. The angular unconformity in the northwest is shown in the photo (c) taken from the Kashi Basin Thrust footwall at the Kekتامu section (Figure 8). Paleozoic strata are intensely deformed prior to Cretaceous deposition. In contrast, the Paleozoic strata in the southeast are disconformable below the Tertiary strata, implying little or no deformation prior to deposition.

These shale-rich strata in the Kashi region form at least 1000 m of shale-dominated mélange (Figure 4b).

[14] Unconformably overlying the Paleozoic strata, but only in the western part of the study area, is the distinctive pink, purple, and orange siltstone, sandstone, and conglomerate of the Cretaceous Kezilesu Formation [Jia *et al.*, 2004; Yin *et al.*, 2002]. Weak shale beds within this formation may act as local detachment horizons where the Cretaceous beds are thrust over Tertiary rocks at many locations. These strata are more than 200 m thick at the western edge of the study area, but thin eastward and are not preserved beyond 75.7°E longitude (Figures 2 and 3a). The Cretaceous units lie disconformably below the Tertiary strata, implying that little or no deformation occurred between the late Cretaceous and early Neogene (Figure 4b). This obvious disconformity above the Cretaceous strata represents the regional erosion surface observed at many locations in the Tian Shan [Abdrakhmatov *et al.*, 2001].

[15] Thin remnants (10–40 m) of Eocene marine shale and fossiliferous limestone, respectively, are preserved locally disconformably above the Cretaceous strata. The base of the limestone is brecciated and has foliation and asymmetric folds that indicate north directed displacement subparallel to bedding. This section has likely been thrust north above the Cretaceous strata along a bedding parallel fault.

[16] The Wuqia Group makes up the lowest part of the Neogene. The group is made up of four units: units A, B, C, and the Pakabulake formation (Figure 3a). The base of the Wuqia group is composed of both units A and B. Unit A consists of 200–250 m of pale yellow, poorly consolidated siltstone, sandstone, and conglomerate interpreted as meandering river channels within an aggrading floodplain. These strata, although confined to the northern foreland, are laterally continuous with unit B to the south that consists of a 300-m-thick section of well-bedded, reddish-brown, gypsiferous siltstone and sandstone. Unit B is interpreted as laterally extensive, shallow lacustrine or marginal-lake deposits that can be traced more than 100 km to the east, south and west (see Yin *et al.* [2002] for southern extent). Both units A and B contain a distinctive, basal 2- to 10-m-thick, orange-brown pebble conglomerate with well-rounded chert pebbles. These units provide a useful marker bed within the northern and medial basins. Magnetostratigraphy brackets the age of units A and B between ~17.5 and 14.9 Ma [Heermance *et al.*, 2007]. Separated from unit B by a sharp contact above a 2-m continuous sandstone bed, unit C consists of pale green siltstone and multihued red mudstone whose lower half consists of ~100 m of pale green silt with 50% gypsum beds up to 1 m thick. The upper half of unit C consists of 100 m of dark red silt, also containing ~50% gypsum and comprising beds <10 cm thick. The exposed thickness of unit C in the study area is <250 m, yet this formation can be traced throughout the basin and forms another marker horizon. Magnetostratigraphic data reveal that the gypsiferous unit C spans from ~14.9 to 13.7 Ma [Heermance *et al.*, 2007]. The upper part of the Wuqia Group is the Pakabulake Formation that consists of at least 2000 m of interbedded siltstone with discontinuous sandstone beds up to 10 m thick. Locally, the Pakabulake Formation is gypsiferous, and the formation is interpreted as a low-gradient, meandering fluvial system that began aggrading circa 13.7 Ma [Heermance *et al.*, 2007].

[17] The Atushi Formation conformably overlies the Wuqia Group and consists of up to 4000 m of interbedded tan sandstone, siltstone, mudstone, gypsum (thin interbeds <10 cm), and rare pebble conglomerate (increasing near top of section). Deposition of the Atushi Formation occurred after ~5.3 Ma at rapid rates of up to 800 m/Ma [Chen *et al.*, 2002; Heermance *et al.*, 2007]. These strata are similar in appearance to the Pakabulake Formation within the Wuqia group, but are distinguishable by their lighter color. Similar to the Pakabulake Formation, the Atushi Formation is interpreted as meandering, low-gradient fluvial and floodplain facies.

[18] The Xiyu Conglomerate caps almost all sections within the Kashi Basin and represents a time-transgressive,

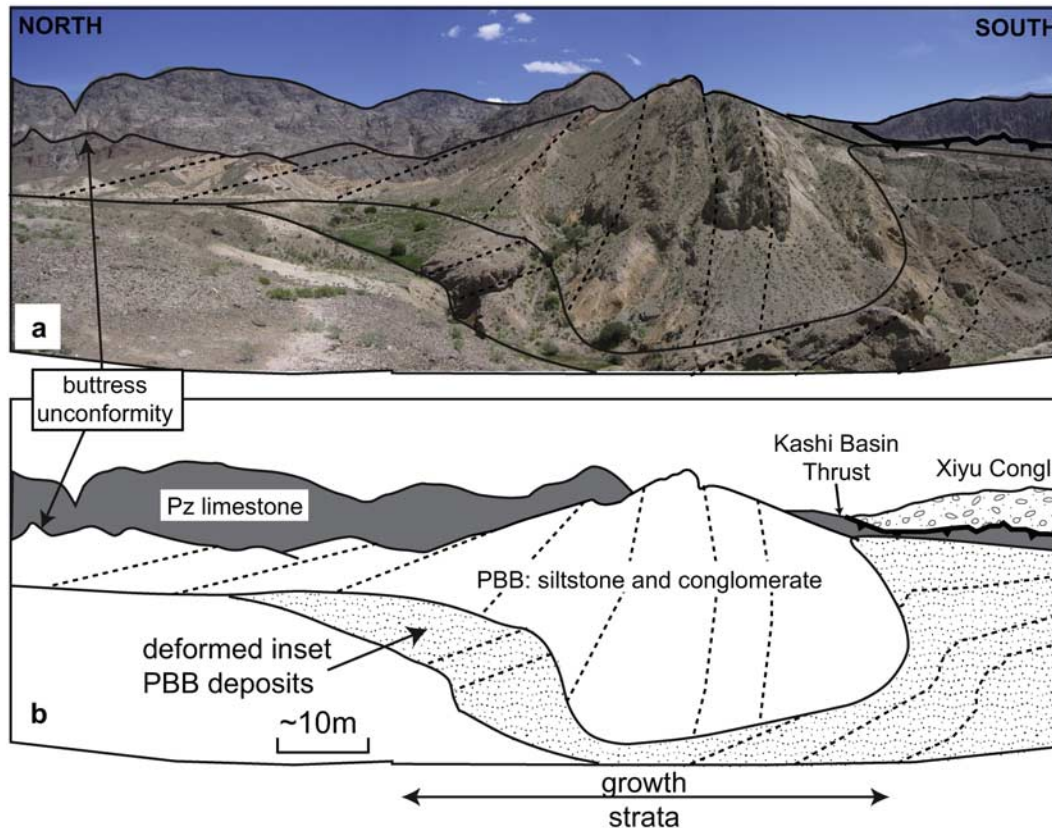


**Figure 5.** (a) Photo mosaic view toward the east of Piggyback Basin sediments (PBB). (b) Line drawing of the image. Fluvio-lacustrine deposits of the PBB lie unconformably above Paleozoic sedimentary rocks. This buttress unconformity is visible at the upper left of the photo. Dashed lines highlight the bedding dips and show bedding progressively steepens toward the south. Inset fill terraces (patterned area in Figure 5b) with similar PBB lithology are less deformed but still dip north opposite to the prevailing river thalweg gradient and represent growth strata within these deposits. Location of image is shown in Figure 6.

southward prograding gravel wedge derived from the uplifted range front [Heermance *et al.*, 2007]. As such, the conglomerate is observed stratigraphically lowest in the northern basin (Figure 3a), where magnetostratigraphy places an age of  $15.5 \pm 0.5$  Ma on its base and large megaclasts and debris flow facies are interpreted to be derived from locally high-relief topography [e.g., Blair and McPherson, 1999]. In contrast, the conglomerate in the southern foreland is less than 100 m thick, has been dated at less than 1.0 Ma, and consists of well-rounded and well-sorted braided fluvial facies [Heermance *et al.*, 2007]. Overall, the Xiyu Conglomerate represents syntectonic deposition coeval with uplift along the margins and within the Kashi foreland.

[19] North of the thick Neogene strata, the Piggyback Basin Formation (PBB) consists of less than 200 m of siltstone, sandstone and conglomerate that mantles and overlies the Paleozoic and Tertiary strata (Figures 2 and 3a). These rocks are in buttress unconformity with the Paleozoic strata (Figure 5) and are interpreted to represent deposition behind structural uplifts in the foreland basin wedge-top [e.g., Decelles and Giles, 1996]. Stratigraphi-

cally and lithologically these strata are similar to the middle Pleistocene Wusu Formation, a thin (<200 m) conglomerate that lies unconformably above the Xiyu Conglomerate along the northern margin of the Tian Shan [Sun *et al.*, 2004]. The discontinuous occurrence of these strata within local topographic depressions makes a regional correlation for this formation speculative. These strata are thickest along their southern boundary, where bedding rapidly steepens southward, and are interpreted as growth strata above an underlying structure (Figure 5). Locally the PBB overlie the steeply dipping Xiyu Conglomerate in angular unconformity, suggesting they are much younger than the 15.5 Ma age for the Xiyu Conglomerate at its northern extent. The presence of strongly north tilted inset terrace deposits indicates that deformation has persisted until recent times.

#### 4. Structures and Shortening

[20] This study mapped  $\sim 6500$  km<sup>2</sup> of the Kashi foreland between 1999 and 2005, with special attention paid to structural deformation of Tertiary strata. Field mapping

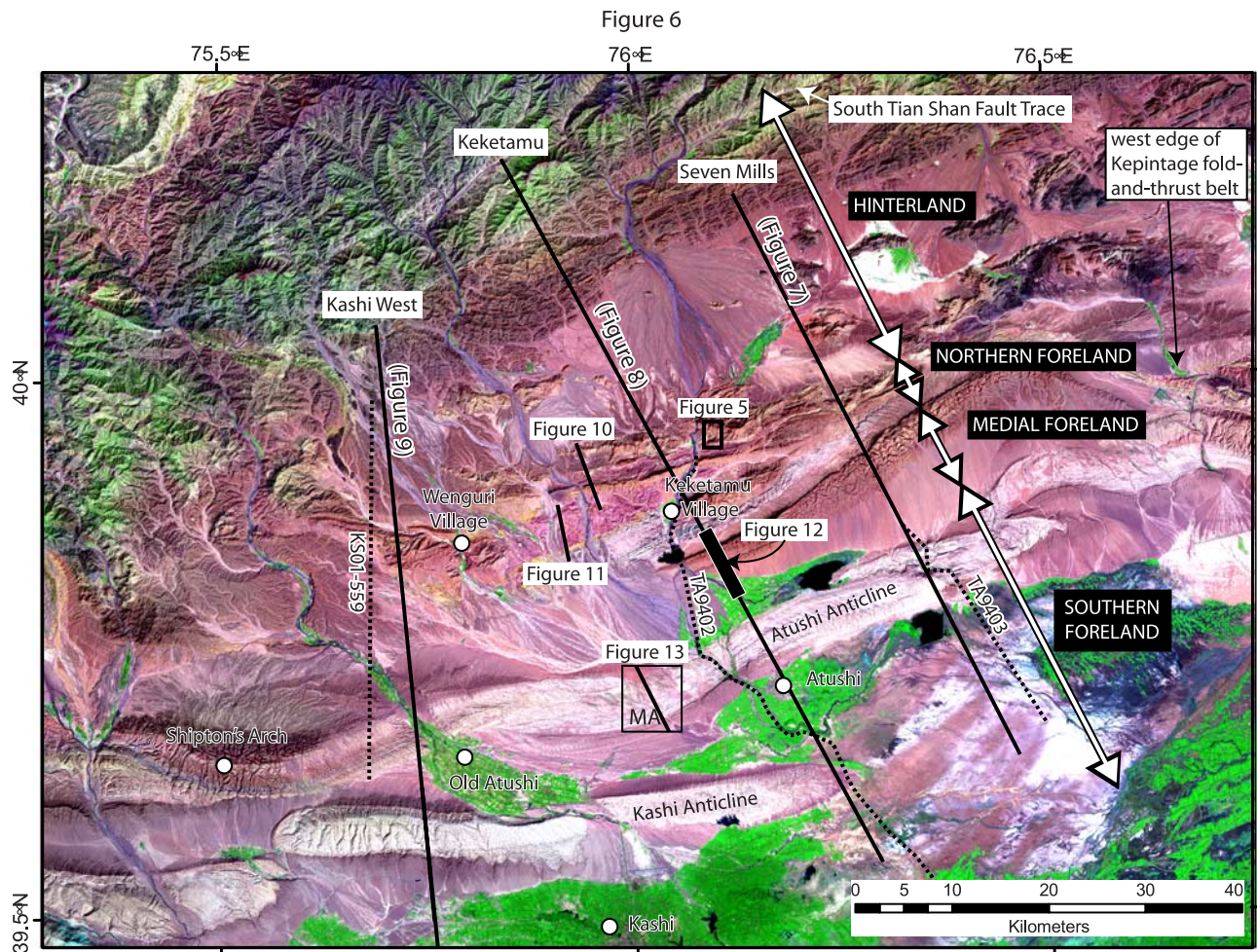


**Figure 6.** Landsat image of the Kashi foreland. The geomorphic expression of basin structures is labeled (e.g., Atushi Anticline). The NW-SE extent of foreland zones (hinterland, northern, medial, and southern) is indicated by the arrows on the right. White circles indicate the locations of major landmarks and towns. Solid black lines indicate the cross sections described in this paper, and dotted lines are the seismic lines used to interpret subsurface structures within each section. Locations of Figure 5, Piggyback Basin strata; Figure 10, Kashi Basin Thrust; Figure 11, Kuyiluke cross section; Figure 12, Keketamu Growth Strata; and Figure 13, Middle Atushi are indicated.

was combined with satellite imagery and, where available, air photos to trace the lateral continuity of bedding and structural lineations. Deformation within the Paleozoic strata was mapped at a reconnaissance level because the age of this deformation is unconstrained over the last 400 million years. Instead, this study focuses on recent deformation history of the Tian Shan observed within the Neogene foreland deposits dated <20 Ma by magnetostigraphy [Heermance *et al.*, 2007]. For simplicity, deformation is divided into four overlapping zones that are described from north to south: (1) hinterland, (2) northern foreland, (3) medial foreland, and (4) southern foreland (Figure 6).

[21] Geologic surface data were combined with proprietary seismic lines provided by PetroChina, Ltd. to construct three balanced geologic cross sections across the Kashi

foreland. These sections are the Seven Mills (Figure 7), Keketamu (Figure 8), and Kashi West (Figure 9) cross sections that are spaced 20 and 35 km apart from east to west across the basin, respectively (Figure 6). Cross sections were constructed to minimize line length, particularly where erosion has removed the higher structural levels. The sections were balanced from the basal Tertiary contact and various stratigraphic levels above this. Seismic lines were time-migrated by PetroChina, and approximate depth conversions for the seismic sections were calculated using the velocity profile for the Kashi foreland provided by PetroChina (Table 1). Depth calculations were made by multiplying the average velocity above any two-way traveltime and dividing by two. Despite errors in our depth calculations or the velocity model, as well as unknown seismic

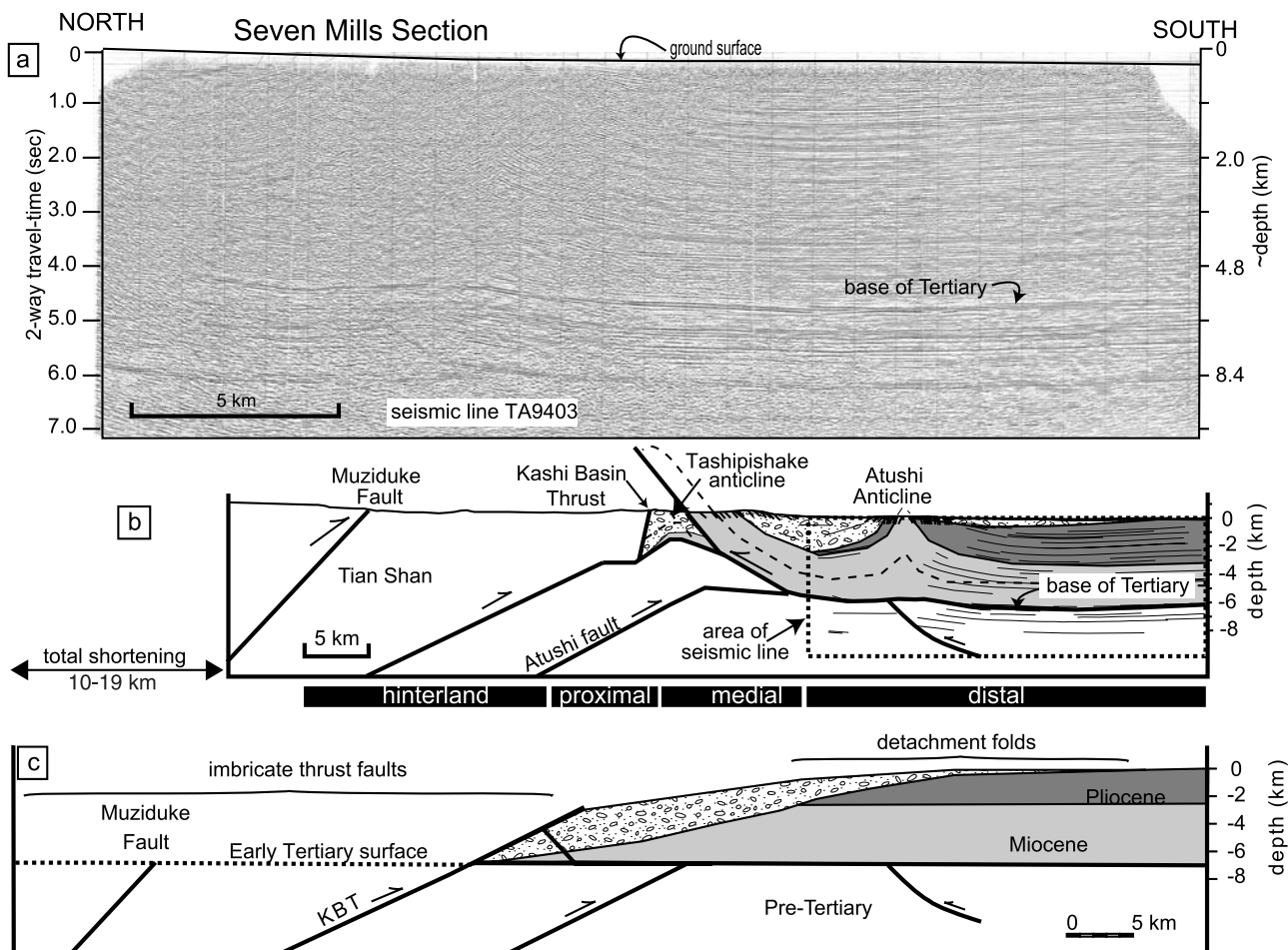


**Figure 7.** Cross-section interpretation and sequential reconstruction for the Seven Mills section. Heavy black lines are faults. The basal detachment is located within a few hundred meters of the Tertiary basal strata. (a) Uninterpreted, time-migrated seismic line TA 9403. Approximate depth conversions based on the depth profile provided by PetroChina (Table 1) are shown at right. (b) Balanced geologic cross-section interpretation. Line drawing of seismic data was converted to depth. The base of the Tertiary shows up as the strong reflector at  $\sim 4.8$  s ( $\sim 6$ -km depth). Area of seismic section is shown as the dotted box. (c) Reconstructed cross section.

migration errors for which we have no control, these seismic lines nevertheless provide valuable constraints on subsurface geometry that would be otherwise difficult to infer on the basis of surface data alone. Thus, these cross sections provide new and more reliable interpretations of the Kashi foreland than have previously been published.

#### 4.1. Methods

[22] Shortening estimates are based primarily on line length, which is calculated by subtracting the horizontal linear distance between two points from the total length of the deformed stratigraphic horizon between those points. Where the fault dip and stratigraphic thickness of footwall deposits that are cut by the fault are known, or the fault dip and exhumation of the hanging wall are known, the minimum shortening is calculated as the product of the cotangent of fault dip with either the stratigraphic thickness cut by the fault or the vertical exhumation caused by the fault.

Both calculations require reconstruction of the original fault geometry and assume planar faults. Shortening is presented as a range based on plausible minimum and maximum values. Although it is impossible to know the exact shortening and errors involved in our estimate, the age range presented accounts for a variety of interpretations within our known shortening constraints, and significantly improves the understanding of structural shortening in the region.

[23] A third way for determining shortening across the detachment folds is via excess area methods after *Epard and Groshong* [1993]. This method assumes that area is conserved within a cross section above a detachment fold. A plot of the area confined below a stratigraphic horizon versus a reference level gives a slope that is equal to the total shortening across the fold. Although assumptions about conservation of area may not be appropriate given the gypsiferous detachments, these shortening estimates nevertheless give alternatives to compare with line length

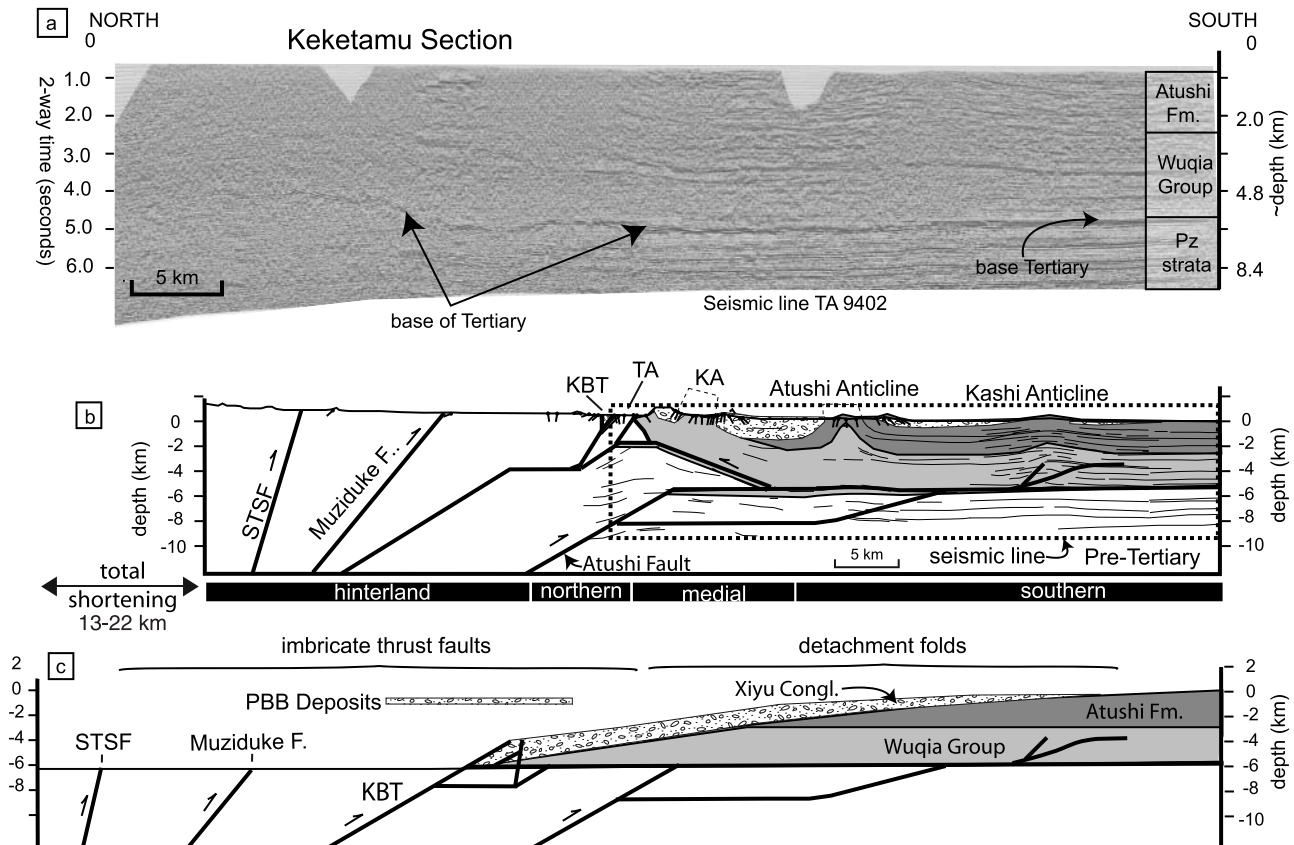


**Figure 8.** Cross-section interpretation and sequential reconstruction for the Keketamu section. Heavy black lines denote interpreted faults and detachment horizons. KBT, Kashi Basin Thrust; TA, Tashipishake Anticline; KA, Keketamu Anticline. (a) Uninterpreted, time-migrated seismic line TA 9402. Approximate depth conversions based on the depth profile provided by PetroChina (Table 1) are shown at right. (b) Balanced geologic cross-section interpretation. Line drawing of seismic data was converted to depth. The base of the Tertiary shows up as the strong reflector at  $\sim 4.8$  s ( $\sim 6$ -km depth). (c) Reconstructed cross section.

estimates that have been shown to be different from actual shortening because of layer parallel, heterogeneous pure shear between stratigraphic layers [Gonzalez-Mieres and Suppe, 2006]. Excess area or similar techniques have been successfully applied to shortening calculations in our study area [Chen *et al.*, 2007; Scharer *et al.*, 2004] to determine shortening along the Kashi and Atushi folds, as well as in other parts of the Tian Shan [Daeron *et al.*, 2007; Gonzalez-Mieres and Suppe, 2006]. We combine new line length estimates with previous conclusions from the Kashi and Atushi folds to determine overall shortening across the Kashi foreland.

[24] Age estimates throughout this study are derived primarily from magnetostratigraphy of the foreland strata [Heermance *et al.*, 2007]. The age of each sedimentation rate change is inferred from the break in slope on the age versus depth plot (Figure 3b). Errors indicated for growth strata and sedimentation rate changes incorporate the range between the two polarity reversals that span the location of either the base of growth strata or the change in sedimentation rate. Details of error analyses for the thermochrono-

logic data and foreland stratigraphy are included in the papers that developed these dates [Heermance *et al.*, 2007; Sobel *et al.*, 2006].

#### 4.2. Hinterland

[25] The northernmost region of the Kashi foreland fold-and-thrust belt is the hinterland, and includes the South Tian Shan Fault (also called Maidan Fault [Chen *et al.*, 2002; Scharer *et al.*, 2004]), the Muziduke Fault, and the broad, low-relief region exposed south of the Muziduke Fault (Figure 6). This entire region is dominated by Paleozoic bedrock with some Quaternary alluvial fans deposited across low-lying areas. The South Tian Shan Fault (STSF) forms the northern boundary of the hinterland and is recognized by a distinctive lineation that trends  $N60^{\circ}E$  that juxtaposes metamorphic rocks in the hanging wall with unmetamorphosed Paleozoic limestone in its footwall. Access to the STSF is limited because of proximity to the international border between China and Kyrgyzstan, but where observed, the fault dips  $74^{\circ}$  north. North of the South Tian Shan Fault lies rugged, mountainous terrain marked by

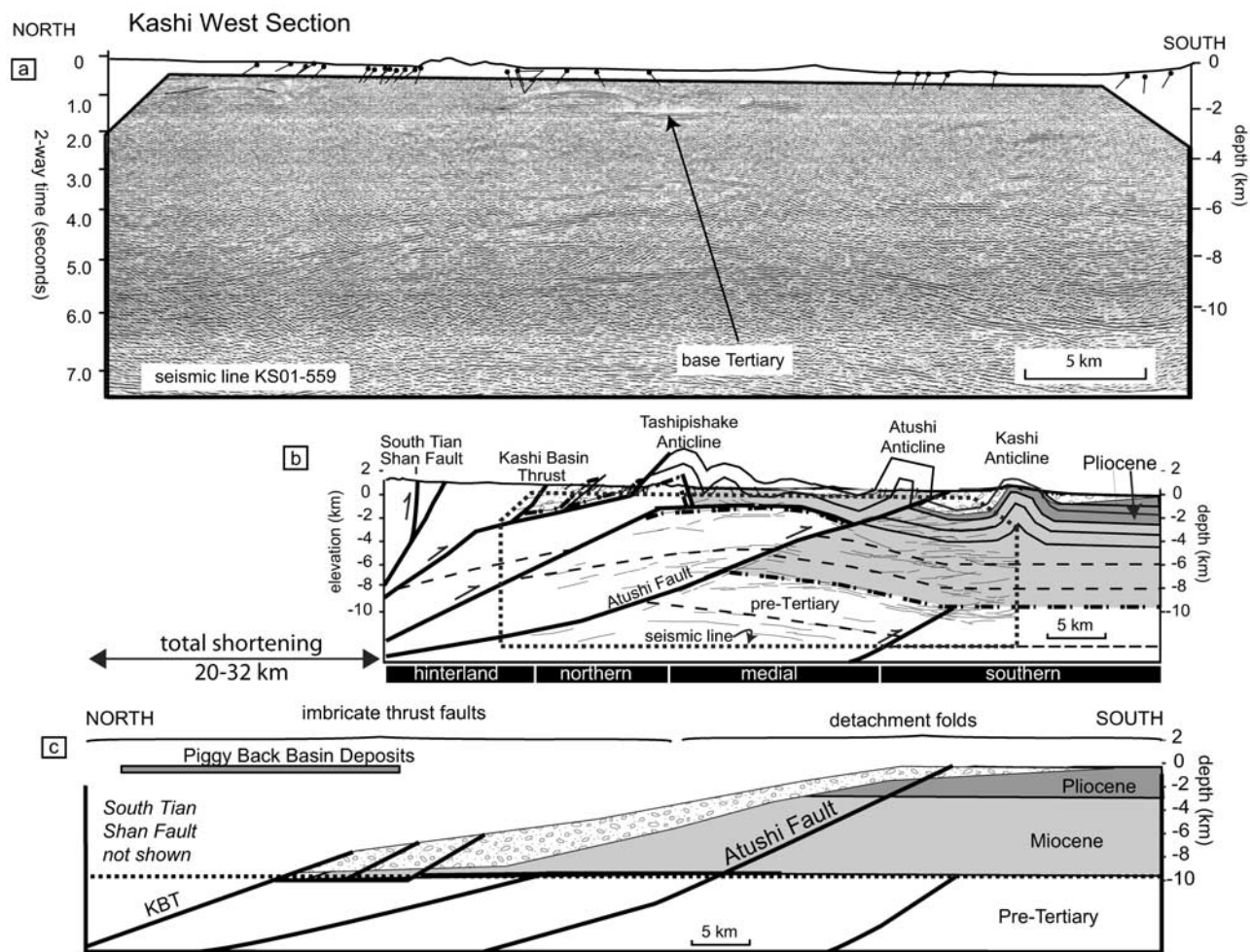


**Figure 9.** Kashi West cross-section interpretation. (a) Seismic line KS01-559 (shown in Figure 6). Data and velocity profile (Table 1) are from PetroChina. (b) Balanced cross section with seismic line-drawing interpretation. The foreland regions (hinterland, northern, medial, and southern) are shown. Black lines are faults, and dashed lines indicate bedding. The area covered by the seismic data is shown. (c) Reconstructed cross section showing the original fault locations and stratigraphic thickness.

incised river canyons and glaciated valleys, whereas south of the fault the terrain is marked by broad alluvial plains pierced by resistant bedrock outcrops. The STSF is interpreted as the range-bounding fault because of the sharp geomorphic contrast across it and because it is the northernmost structure identified along the southern flank of the Tian Shan in this region [Sobel *et al.*, 2006].

[26] The Muziduke Fault is located ~15–20 km south of and subparallel to the STSF, where it cuts Paleozoic strata (Figure 2) [Chen *et al.*, 2001; Xinjiang Bureau of Geology and Mineral Resources, 1993]. Within much of the Kashi foreland, the fault trace is buried by alluvium, but the Muziduke Fault may correlate with an imbricate thrust fault within the Kepintage thrust zone east of the Kashi foreland [Allen *et al.*, 1999; Yin *et al.*, 1998].

#### 4.2.1. Deformation Age

[27] Thermochronology defines fault activity as late Tertiary for both the South Tian Shan Fault and Muziduke

Fault. Apatite fission track ages of 20–25 Ma from the hanging wall of the STSF and Muziduke Fault, combined with unreset samples within the footwall of each fault respectively, suggest differential exhumation beginning at 20–25 Ma [Sobel *et al.*, 2006]. Unreset apatite fission track samples elsewhere in the hinterland are >80 Ma and are interpreted to represent either earlier tectonic phases or limited erosional exhumation during the Miocene to recent. We interpret the 20–25 Ma samples to represent the initiation of Tertiary deformation along the southern Tian Shan.

#### 4.2.2. Shortening

[28] Shortening is more difficult to constrain across these hinterland structures because hanging wall cutoffs have been eroded and the Paleozoic stratigraphy is not well known [Carroll *et al.*, 1995]. By assuming a geothermal

**Table 1.** Seismic Velocity Profile of Kashi Foreland Provided by PetroChina<sup>a</sup>

Two-Way Traveltime (sec)	Velocity (m/s)
0	1640
300	1640
500	1740
700	1850
900	1960
1200	2130
1500	2310
1800	2480
2100	2650
2500	2875
3000	3120
3500	3360
4000	3575
4500	3790
5000	3975
5500	4120
6000	4240
6500	4340
8000	5500

<sup>a</sup>The two-way traveltime was used to calculate the depths of seismically interpreted stratigraphic horizons.

gradient of  $22 \pm 3^\circ\text{C}$  per kilometer depth [Sobel and Dumitru, 1997; Zhang, 1989], a  $10^\circ\text{C}$  average surface temperature, and  $105 \pm 5^\circ\text{C}$  closure temperature for the apatite [Sobel et al., 2006], the reset ages in the hanging walls have been exhumed 3.5–5.3 km since 20–25 Ma, whereas unreset samples in the footwall have been exhumed <3.3 km. These calculations suggest differential rock uplift across each of these faults in the late Oligocene to early Miocene, followed by broad regional exhumation, but total exhumation remains unconstrained. Whereas we cannot place useful limits on the total amount of shortening across either the STSF or Muziduke faults,  $\sim 7$  km of total shortening was estimated on each of the equivalent structures in the Kepintage fold-and-thrust belt  $\sim 100$  km to the east [Allen et al., 1999], and may be a good approximation for these northernmost structures in the Kashi Basin.

[29] Growth structures within the Piggyback Basin strata (PBB) indicate more recent deformation of the hinterland. PBB strata typically dip  $\sim 10^\circ$  north but progressively steepen to  $>60^\circ$  along their southern margin within (<1 km) the Kashi Basin Thrust (Figure 5). Inset fill terraces that dip only  $20\text{--}30^\circ$  north are juxtaposed and onlap with the  $60^\circ$  dipping beds. Both the fill terraces and PBB strata consist of similar conglomerate lithologies and may be equivalent deposits. Progressive tilting of this region combined with deposition on the rotating fold flanks thus produced growth strata represented by the steepening dips [Riba, 1976]. Limited exposures of the PBB deposits prohibit shortening determinations for these Upper Cenozoic strata. This region, however, has clearly been folded during deposition of the PBB, suggesting deformation occurred in the hinterland well after initial uplift and shortening across the South Tian Shan and Muziduke faults.

### 4.3. Northern Foreland

[30] The Kashi Basin Thrust (KBT) bounds the northern foreland where it juxtaposes Paleozoic or Cretaceous hanging wall strata with Tertiary conglomerate in its footwall. Previously called the Tuotegongbaizi/Aerpaleike Fault [Allen et al., 1999; Scharer et al., 2004], the KBT can be traced as a single continuous strand for  $\sim 50$  km between  $75.8$  and  $76.3^\circ\text{E}$  longitude, although in places, synthetic imbricate faults disrupt its proximal footwall. We do not trace the fault west of our mapped area at  $75.25^\circ\text{E}$  longitude, but Landsat images suggest it continues westward. Toward the east, an imbricate thrust fault along strike and within the Kepintage thrust zone may correlate with the KBT [Allen et al., 1999; Yin et al., 1998]. Where exposed, the KBT is subvertical to overturned. Steeply north dipping ( $60\text{--}90^\circ$ ) Xiyu Conglomerate in the footwall implies that this area has been tilted north after initial faulting. Restoring these footwall strata to horizontal suggests an original thrust dip of  $0\text{--}30^\circ$  north (Figure 10b). Where observed in outcrop, fault gouge is limited to a narrow, less than 0.5-m-thick zone of sheared gray shale with striae that indicate pure dip-slip movement. Paleozoic strata in the hanging wall consist of intensely deformed, isoclinally folded Paleozoic shale mélangé, except for at the Kashi West section where Cretaceous rocks are observed.

#### 4.3.1. Deformation Age

[31] The initiation of slip of the Kashi Basin Thrust is constrained with two data sets: reset apatite fission track (AFT) ages in its hanging wall and magnetostratigraphy of syntectonic strata in its footwall. Paleozoic sandstone samples collected  $\sim 100$  m north of the fault yielded a reset AFT date of  $18.9 \pm 3.3$  Ma [Sobel et al., 2006], interpreted to define the initiation of hangingwall uplift, erosion, and cooling at this locality. The beginning of local deposition of the Xiyu Conglomerate in the footwall of the KBT at  $15.5 \pm 0.5$  Ma is interpreted as a direct response to the initiation of thrusting [Heermance et al., 2007]. Prior to  $15.5 \pm 0.5$  Ma, deposition south of the KBT was slow ( $0.05\text{--}0.08$  mm/a, Figure 3b) and consisted of fine-grained lacustrine or fluvial strata. At  $16.3 \pm 0.3$ , Ma, a sharp increase in sediment accumulation rates is inferred at two localities within the basin (Figure 3b) and is closely followed by the appearance of rockfall and debris flow lithofacies in the footwall of the KBT within one kilometer of the fault [Heermance et al., 2007]. The combination of coincident increased sediment accumulation rates at two locations in the footwall of the KBT, indirect evidence of newly developed, locally high relief in the hanging wall as a source for incipient Xiyu Conglomerate lithofacies, and cooling in the hanging wall all suggest an initiation of uplift at  $16.3 \pm 0.3$  Ma for the Kashi Basin Thrust.

#### 4.3.2. Shortening

[32] Shortening estimates across the KBT are based on the thickness of syntectonic footwall strata, initial fault dip, and thermochronology of the hanging wall. At least 500 m of footwall strata are cut by the KBT, and thus by reconstructing the original fault dip to  $30^\circ$  and the footwall strata to horizontal, we calculate a minimum of  $\sim 800$ -m shortening across this fault. No hanging wall cutoffs are preserved to

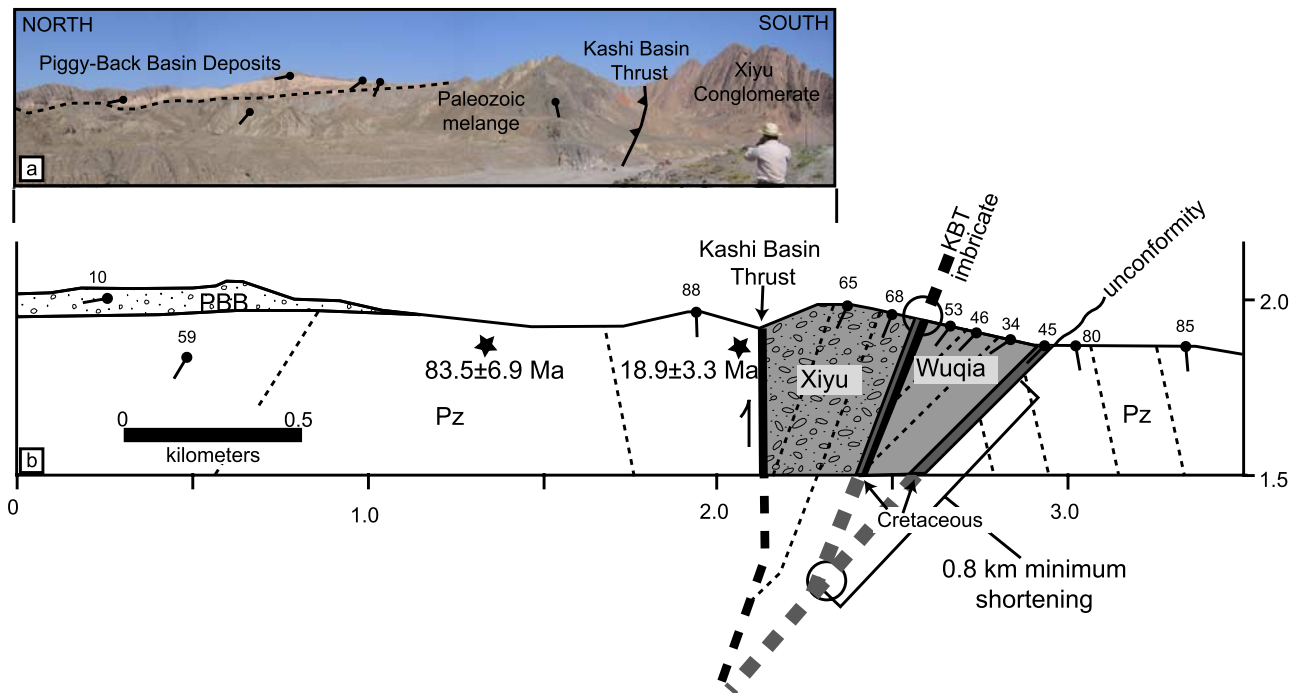


**Figure 10.** (a) Photograph and (b) cross section across the Kashi Basin Thrust and the hinterland part of the study area. Location is shown in Figure 6. Extrapolation of planar fault ramps and bedding dips to depth allows us to calculate minimum shortening across the KBT imbricate. The location and ages of the apatite fission track samples (stars) from Sobel *et al.* [2006] are shown in the hanging wall of the Kashi Basin Thrust. Shaded areas are labeled Neogene and Cretaceous strata.

estimate total uplift. More than 500 m of debris flow facies conglomerate in the footwall, however, requires locally high topography at the time of deposition. Therefore we place a minimum surface uplift of >1000 m in the hanging wall and thus >1600 m of shortening are estimated for the KBT. Maximum shortening is constrained by the apatite fission track (AFT) ages in the hanging wall. The reset sample ( $18.9 \pm 3.3$  Ma) is located  $\sim 100$  m into the fault hanging wall and a second, unreset ( $83.5 \pm 6.9$  Ma), structurally higher sample is located  $\sim 800$  m further north (Figure 10) [Sobel *et al.*, 2006]. The close juxtaposition of the reset age with an unreset age for the same lithology suggests that the base of the partial annealing zone ( $\sim 110^\circ\text{C}$  at 4-km depth) was located between these samples within the KBT hanging wall. Thus, by assuming the same geothermal gradient as the hinterland, no more than  $\sim 4$  km of exhumation occurred since initiation of the fault at  $18.9 \pm 3.3$  Ma, and given a reconstructed fault dip of  $30^\circ$ , shortening was 7 km (Table 2).

[33] Discontinuous, synthetic north dipping thrust faults occur within the Kashi Basin Thrust footwall where they place Cretaceous siltstone over Tertiary strata, resulting in a thick succession of stacked stratigraphic sequences. The imbricate structure within one kilometer of the KBT at the Keketamu section (Figure 10b) is responsible for some rotation of the KBT above the fault ramp, whereas further rotation likely occurred later above a deeper structure. Two imbricate thrust faults are observed in the footwall of the KBT at the Kashi West section (Figure 9b). Although hanging wall cutoffs above these imbricate faults have been

eroded, the Tertiary basal unconformity provides an excellent marker to determine minimum shortening. In each case, the disconformity between the Cretaceous and Tertiary is preserved above and subparallel to the fault, and implies detachment within the thin (<200 m) Cretaceous strata. By reconstructing fault dip to  $30^\circ$  and using a minimum Tertiary thickness of 500 m, at least 800 m of shortening, but likely much more, has occurred above the footwall imbricate at the Keketamu section (Figure 10). Therefore, we estimate 1- to 2-km shortening at this site (Table 2). At the Kashi West section, two footwall imbricate faults occur within 6 km of the KBT. On the basis of our balanced cross section at Kashi West (Figure 9), the depth to the detachment horizon is 2–3 km. Line length calculations indicate  $\sim 4$  km of shortening across the two imbricate thrusts. Alternatively, the Tertiary strata thickness of footwall deposits are  $\sim 2$  km for both structures, and using the reconstructed fault dips of  $30^\circ$ , we can calculate a maximum shortening of 7 km. Line length estimates are lower than thickness-based estimates because the line length method minimizes shortening in the eroded hanging wall, such that the entire length of rupture through the footwall strata may not be accounted for. Nevertheless, we estimate combined shortening of 4–7 km across these imbricate structures at Kashi West (Table 2).

#### 4.4. Medial Foreland

[34] The medial foreland comprises the region between the northern foreland and the Atushi Anticline (Figure 6).

**Table 2.** Table of Shortening Magnitude for Each of the Kashi Foreland Structures<sup>a</sup>

Structure	Kashi West		Keketamu		Seven Mills		Method for Age Determination
	Shortening Range	Initiation Age (Ma)	Shortening Range	Initiation Age (Ma)	Shortening Range	Initiation Age (Ma)	
				<i>Hinterland</i>			
South Tian Shan Fault	>0	20–25	>0	20–25	>0	20–25	apatite fission track [Sobel <i>et al.</i> , 2006] apatite fission track [Sobel <i>et al.</i> , 2006] crosscutting relationships and magnetostratigraphy
Muziduke Fault	>0	20–25	>0	20–25	>0	20–25	
Piggyback Basin	>0	0.78–14	>0	0.78–14	>0	0.78–14	
				<i>Northern Foreland</i>			
Kashi Basin Thrust (KBT)	2–7	16.3 ± 0.5	2–7	16.3 ± 0.5	2–7	16.3 ± 0.5	sedimentation rate increase, reset apatite fission track age [Sobel <i>et al.</i> , 2006] relative
KBT footwall imbricates	4–7	<16.3	1–2	<16.3	na	na	
				<i>Medial Foreland</i>			
Tashipishake Anticline (seismic)	4–5 <sup>b</sup>	13.5 ± 0.1 <sup>b</sup>	2–3 <sup>b</sup>	13.5 ± 0.1 <sup>b</sup>	1–2 <sup>b</sup>	<16.3 <sup>b</sup>	sedimentation rate, facies change, and crosscutting relationships related to Tashipishake Anticline sedimentation rate and growth strata
Back thrust Keketamu folds (surface data)	na	na	na	na	5–6	<16.3	
	4–5	13.5 ± 0.1	4–5	3.9–4.0	na	na	
				<i>Southern Foreland</i>			
Atushi Fault (seismic)	10–12 <sup>b</sup>	na <sup>b</sup>	7–8 <sup>b</sup>	na <sup>b</sup>	8–9 <sup>b</sup>	3.9–4.0 <sup>b</sup>	relative age based on Keketamu fold initiation to west cuts <5.3 Ma strata
Atushi Fault (outcrop)	4–5	<5.3	na	na	na	na	
Atushi Anticline	3–4	>1.4	4–5	1.4 ± 0.3	2–4	1.4 ± 0.3	growth strata growth strata
Kashi Anticline	2–3	1.4 ± 0.3	>0	na	na	na	
Totals		20–32		13–22		10–19	

<sup>a</sup>Italicized estimates are not used in the “Total” calculation because these values are redundant and shortening is accounted for by other structures in the same section (e.g., shortening across the Atushi Fault displacement is equivalent to shortening within the Atushi Anticline). Magnitude ranges and age errors are described within the text.

<sup>b</sup>Seismically interpreted data.

This region consists of east-west trending anticlines and synclines that are locally faulted. Although the overall geometry of the medial basin is similar along strike, the surface expression varies from a 5- to 10-km-wide zone with short (1–2 km) wavelength folds (Figure 9b) to a narrow (<3 km) zone of localized deformation across a single anticline associated with a south dipping back thrust (Figure 7b). Structural descriptions and along-strike variability are described here.

[35] The northern boundary of the medial basin is defined by the Tashipishake Anticline that extends for more than 50 km subparallel and south of the Kashi Basin Thrust (Figure 2) and forms the apex of the triangle zone geometry of this fold-and-thrust belt [Banks and Warburton, 1986; Couzens and Wiltschko, 1996; Jones, 1996]. Paleozoic strata, similar to that observed in the hanging wall of the KBT, typically core this anticline (Figure 11). The exception is at the Seven Mills section (Figure 7) where only the Xiyu Conglomerate is exposed across the anticline because of the structurally higher position of the fold at this location. The northern anticlinal flank is defined by 30–50° north dipping Cretaceous and Tertiary strata that dip beneath the imbricate thrust faults south of the KBT (Figure 11). The southern

fold flank is generally defined by steep (>60°) to overturned Tertiary strata at the surface. The Tashipishake Anticline is interpreted as a south vergent fault bend fold [e.g., Suppe, 1983] because (1) the southern fold flank is truncated above a subhorizontal detachment horizon, (2) a back thrust along the southern flank is most easily explained by emplacement of a fault bend fold duplex beneath the Tertiary strata [Charlesworth and Gagnon, 1985; Jones, 1996], and (3) north dipping faults along the fold’s southern flank have displacements of less than 0.5 km that are too small to be responsible for the more than 6 km of rock uplift observed north of the fold. In the Kashi West section, a 30° north dipping, concave-up fault ramp is interpreted below the hinterland region and bends along a seismically interpreted detachment at the base of the Tertiary strata at 2-km depth (Figure 9). Preserved fluvial terraces at Kuyiluke are north dipping and progressively steepen with increasing height above the active channel, consistent with a curved fault ramp at depth (Figure 11c) [Amos *et al.*, 2007]. This lower fault ramp bends along the subhorizontal base of the Tertiary contact, and a fault bend fold forms above this bend. Although it is not imaged seismically at the Keketamu or Seven Mills sections at 1- to 2-km depth, the upper

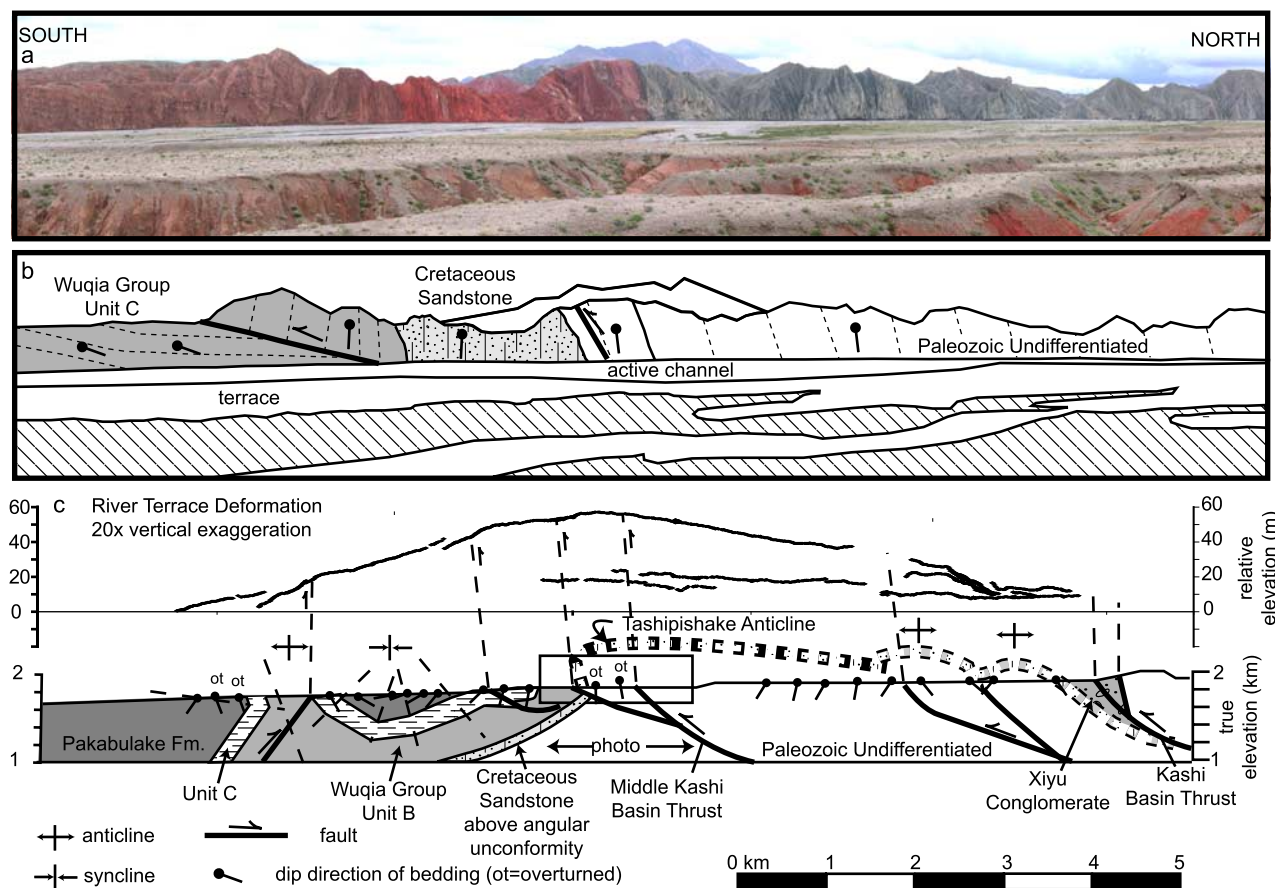


**Figure 11.** (a) Photomosaic of the Kuyiluke section. (b) Line drawing. (c) Terrace profile and geologic cross section across the Kuyiluke region shown in Figure 6.

detachment is inferred at approximately the same depth beneath the Tashipishake Anticline as at Kashi West (2 km). The fault ramp north and below the Tashipishake Anticline, however, connects the base of the Tertiary with a lower detachment at  $\sim 4$ -km depth that originates from the Kashi Basin Thrust (KBT). Translation of the KBT across and above the fault ramp that forms the Tashipishake Anticline further rotates the KBT to its subvertical geometry at these eastern localities. Although the upper detachment levels appear the same, the geometry of the basement faults varies from a curved, deep ramp at Kashi West to a more shallow, ramp-flat-ramp geometry in the east.

[36] Faulting and folding both within and south of the Tashipishake Anticline accommodate shortening within the overlying strata that balances that along the lower fault ramp. A major back thrust is observed at both the Seven Mills and Kashi West sections, defined by fault breccia and sheared, foliated shale along the southern flank of the Tashipishake Anticline. The back thrust is confined to within 100 m of the base of the Tertiary strata, and it juxtaposes a more than 3-km-thick homoclinal sequence of Wuqia Group with the lower part of the Xiyu Conglomerate at the Seven Mills section (Figure 7b). In contrast, no back thrust is observed at the Keketamu section, where a series of short-wavelength (not shown on the regional cross section,

Figure 8), faulted detachment folds occur in front of the Tashipishake Anticline, including the Keketamu Anticline that marks the southern margin of the medial basin and extends more than 50 km west-east. These folds are cored by the gypsiferous Wuqia group, are locally isoclinal, and are interpreted to represent north vergent fault-related folding above the gypsiferous basal units of the Tertiary strata. Shortening within the Tertiary strata in the medial basin is thus accommodated either across a south dipping back thrust or detachment folds south of the Tashipishake Anticline. In addition, north dipping faults cut the core and southern flank of the Tashipishake Anticline, such as observed at the Kuyiluke region (Figure 11c). These faults, however, have displacements less than 0.5 km and could not have provided the slip to elevate the base of the Tertiary over 6 km relative to the southern foreland.

#### 4.4.1. Deformation Age

[37] Deformation ages within the medial foreland are constrained by crosscutting relationships, deposition rate changes, and growth strata. A more than threefold fold increase in sedimentation rate from 0.12 to 0.43 mm/a is observed at  $13.5 \pm 0.1$  Ma and corresponds to a lithologic change from gypsiferous lacustrine deposits to more lake-marginal and fluvial deposition of the Pakabulake Formation (Figure 3b). Although sedimentation rate can increase

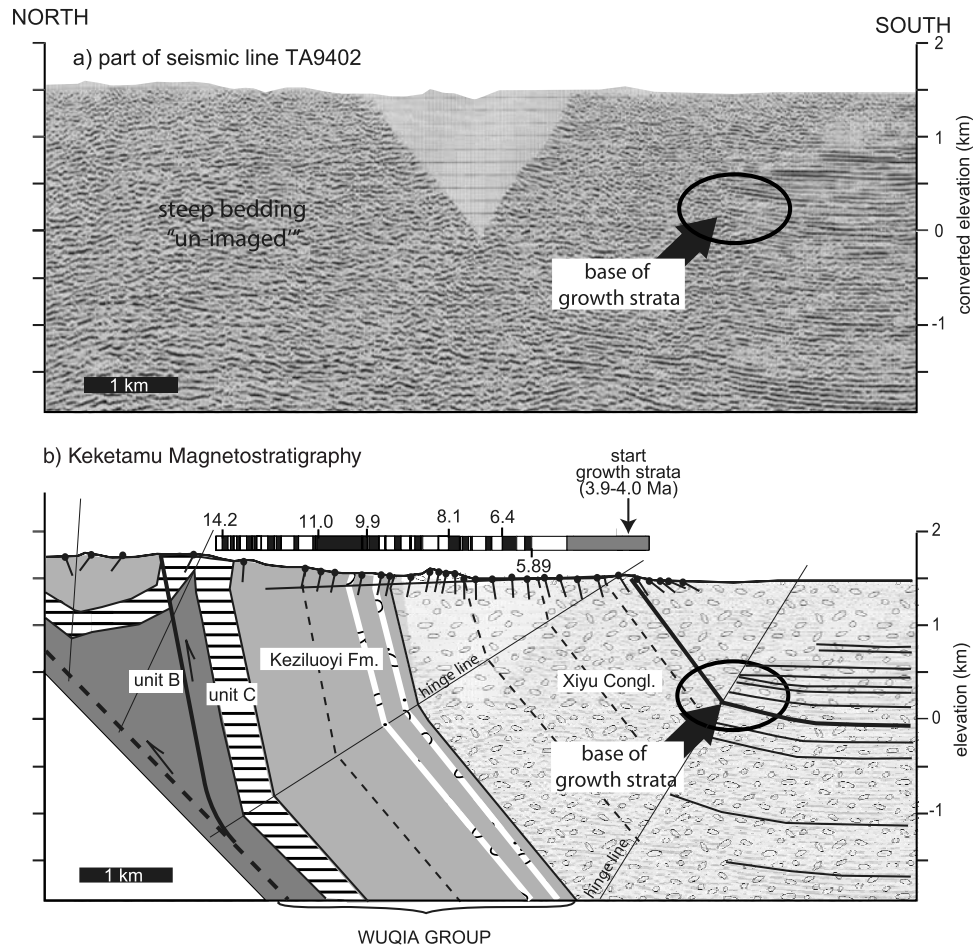


**Figure 12.** Growth strata interpretation along the southern flank of the Keketamu Anticline. Location is shown in Figure 6. (a) Enlarged section of seismic line TA9402 that shows the angular unconformity and onlap relationship of growth strata to the fold. (b) Geologic interpretation of the seismic section. Surface data are included, and mappable subhorizontal strata south of the Keketamu fold are drawn in on the basis of seismic data. Hinge lines are shown in the cross section, and growth strata are defined by the fanning dip sequences along the fold flanks. The base of the growth strata is determined by field mapping and from the seismic data where the bed thickness begins to change across the fold. Magnetostratigraphy above the cross section shows normal (black) and reversed (white) magnetic polarity zones and their stratigraphic locations along the southern flank of each fold. Ages are Ma and based on correlation within the Geomagnetic Polarity Timescale [Lourens *et al.*, 2005]. Gray zone within the magnetostratigraphy is a region of poor age correlation and 100-m sample spacing. Extrapolation of the sedimentation rates to the growth strata give an age of 3.9–4.0 Ma.

because of a variety of factors such as increased tectonic subsidence, higher sediment flux, or a change in depositional environment, we interpret this increase to tectonic subsidence resulting from growth of and loading by the Tashipishake Anticline. An abrupt southward jump in the deformation front would account for the rapid change from lacustrine to more proximal fluvial and lake-marginal deposition and for the lack of any deposition above the anticline after 13.5 Ma. Furthermore, we are aware of no major climatic changes toward more erosive conditions at this time to account for a sustained change in sedimentation rate after 13.5 Ma [Clift, 2006; Guo *et al.*, 2002; Métivier and Gaudemer, 1997; Molnar, 2004]. Thus, our evidence

suggests that development of the Tashipishake Anticline began circa 13.5 Ma.

[38] Eight kilometers further south, growth strata are observed along the southern flank of the Keketamu Anticline (Figure 12). The base of growth strata are determined by recognition of an abrupt decrease and fanning of dips unrelated to a fold hinge at the surface. In addition, the base of the growth strata is inferred from our seismic line TA 9402 where onlap relationships and bed thickness changes above the base of the growth strata is observed (Figure 12a). The base of the growth strata could not be dated directly with magnetostratigraphy because of very large (100 m) sample spacing within the coarse conglomerates [Heermance *et al.*,

2007], but is inferred at 3.9–4.0 Ma from extrapolation of the constant  $0.43 \pm 0.1$  mm/a sedimentation rate at the Keketamu section (Figure 3b). This age corresponds with a subtle ( $\sim 15\%$ ) increase in sedimentation rate 12 km farther south above the Atushi Anticline (Figure 3b). We interpret the change in sedimentation rate to result from thrust loading of Paleozoic basement and the initiation of Keketamu folding that generates a proximal source for accelerated deposition above the (future) Atushi Anticline further south.

#### 4.4.2. Shortening

[39] Shortening across the medial basin is determined from displacement of the Tertiary basal unconformity along the upper detachment and from line length shortening estimates across folds south of the Tashipishake Anticline (Table 2). Offset of the base of the Tertiary along the upper detachment beneath the Tashipishake fold decreases linearly toward the east, from 4–5 km at Kashi West to 1–2 km at Seven Mills. As described above, shortening across the fault ramp below the anticline is accommodated within the Tertiary strata via both folding above and south of the fold, and back thrusting along the southern fold flank. At Kashi West, line length shortening for the folds south of Tashipishake Anticline accounts for 4–5 km of shortening that balances shortening below the Tashipishake fold (Table 2). In contrast, at Keketamu and Seven Mills, the folding and back thrusting observed (4–6 km) in the medial basin is greater than the offset across the Tashipishake Anticline (1–3 km). We attribute the extra shortening to contraction across the Atushi Fault, 10 km south of the Tashipishake Fault ramp. Shortening decreases from west to east across the Tashipishake Anticline, thereby implying an eastward plunge of the structure.

#### 4.5. Southern Foreland

[40] The Atushi and Kashi anticlines form the striking geomorphic features that trend east-west and make up the southern zone of deformation across the southern foreland region (Figures 2 and 6). The Atushi and/or Pakabulake Formations are exposed in the cores of both anticlines except in the Kashi West section, where the stratigraphically lower Wuqia group unit C crops out in the core of the Atushi fold. The geomorphology of both folds is dominated by preferential erosion of the weak Atushi and Wuqia Group Formations relative to the more resistant Xiyu Formation, which controls their  $\sim 8$ -km-wide topographic expression. Where erosion has removed the conglomerate or none is present, the topography across the anticlines is subdued. Thus, despite several kilometers of structural relief [Scharer *et al.*, 2004], the geomorphic relief across these folds is modest ( $< 500$  m).

[41] The Atushi Anticline trends  $N70^\circ E$ , stretches for  $> 100$  km across the Kashi foreland, and makes up the northern of the two southern foreland structures. Total structural width of the fold is 10–15 km based on gently dipping ( $5$ – $15^\circ$ ) beds in the subsurface along the flanks of the fold (Figures 7 and 8). The Atushi fold has a box-like geometry [Scharer *et al.*, 2004] with steeply dipping ( $60$ – $90^\circ$ ) fold limbs. The tight box-like shape, variable vergence, and subhorizontal seismic reflectors beneath the fold at the Keketamu and Seven Mills sections suggest the fold is a lift-

off type detachment fold [Mitra, 2002]. Overall, the Atushi Anticline shows an eastward plunge and detachment is inferred to occur between 4- and 6-km depth. At the Kashi West section, however, the Atushi Fault has translated the Atushi Anticline south over gently south dipping foreland strata above a  $20$ – $35^\circ$  dipping convex-up fault (Figure 9b). Slip along the Atushi Fault may initially have been transferred to a footwall flat within the Wuqia Group strata, creating a fault bend fold in the near surface. As displacement increased on the Atushi Fault ramp, this fault eventually cut across the footwall detachment and translated the Atushi Anticline southward, causing tightening of the fold in the process (Figure 9). North and south dipping faults cut the core of the Atushi Anticline near the western limit of the study area where the fold limbs are isoclinal (Figure 2). Although the south dipping thrusts accommodate displacements of less than a few hundred meters, the north dipping thrust uplifts the thick ( $> 2$  km) Xiyu Conglomerate along the north flank of the Atushi Anticline where it forms the erosion-resistant ridge containing “Shipton’s Arch”: a topographic landmark at the ridge crest (Figure 6). The eastern fold termination plunges gently east just south of the Mutule Anticline (Figure 2), where shortening is likely transferred between them.

[42] The Kashi Anticline trends subparallel to the Atushi Anticline ( $N85^\circ E$ ) but extends only  $\sim 60$  km along the southern edge of the fold-and-thrust belt [Chen *et al.*, 2007]. In cross section, the fold forms subdued but rounded topography, and generally has higher average topography than the Atushi fold at any individual cross section perpendicular to fold strike. At the terminations of this doubly plunging anticline, the elongate eastern nose plunges at  $\sim 2^\circ$  into the depositional plain of the Tarim Basin, whereas the blunt western end abruptly terminates between the Mingyao and Atushi anticlines (Figure 2). At the surface along its western half, the anticline exhibits steep limbs with dips of  $50$ – $80^\circ$ , separated by relatively flat dips near the axis [Scharer *et al.*, 2004], which give the fold a box-like shape (Figure 9b). The eastern half forms a broad, gentle fold with  $5$ – $15^\circ$  limbs (Figure 8b). Where we have conducted geologic mapping, discontinuous reverse faulting with displacement of less than 200 m occurs locally along the fold flanks (Figure 2).

[43] The Kashi Anticline is a detachment fold and forms the southernmost deformation within the foreland [Chen *et al.*, 2007; Scharer *et al.*, 2004]. At least two detachment levels are interpreted between  $\sim 3$ - and  $\sim 6$ -km depth in seismic section TA 9402 (Figure 8a). Furthermore, variable vergence along strike, its box-like shape (Figure 9b), and a lack of any major faults along its flanks, support the interpretation of a detachment fold. Folding deforms no less than 6 km of syntectonic, subhorizontal foredeep strata. On the basis of seismic interpretation, strata are discontinuous across a fault ramp and represent a fault bend fold below the upper detachment [Chen *et al.*, 2007]. Above the subhorizontal detachment, strata likely behave as faulted detachment folds with moderate strain (similar to Mitra [2002, Figure 3c]) or detachment folds above a fault bend fold in the basal layer (analogous to *Gonzales-Mieres and*

*Suppe* [2006, Figure 13d]). We therefore interpret the Kashi Anticline as a detachment fold above a distributed detachment zone between 3- and 6-km depth, with strain accommodated below the upper detachment by both faulting and layer parallel shear.

#### 4.5.1. Deformation Age

[44] Growth strata [e.g., *Poblet and McClay*, 1996] are dated with magnetostratigraphy and constrain the initiation of fold growth along the southern flanks of both the Atushi and Kashi anticlines [*Chen et al.*, 2002, 2007]. The growth strata interpretation is based on the fanning dips over short (100–200 m) distances above constant dipping fold limbs (Figure 12), and angular unconformities that suggest offlap during syn-fold sedimentation [*Riba*, 1976]. Furthermore, the base of growth strata is interpreted seismically as the level where beds change from constant thickness to thinner above the fold [*Chen et al.*, 2007]. Initiation of shortening of the Atushi fold is paleomagnetically defined at  $1.4 \pm 0.3$  Ma at the base of growth strata along the Middle Atushi cross section (Figure 13). About 10 km farther east, the oldest growth strata date to  $1.2 \pm 0.1$  Ma and suggest eastward propagation of the Atushi Anticline that is consistent with its eastward structural plunge [*Chen et al.*, 2002]. These dates provide our only precise temporal evidence for the initiation of deformation of the Atushi fold. However, the deeper structural levels exposed at the western end, combined with a tighter (isoclinal) fold geometry, greater shortening, and the overall eastward plunge of the anticline, suggest that deformation likely initiated earlier near the Kashi West section than at the Keketamu section ( $\sim 1.4$  Ma).

[45] Along the Kashi Anticline, ages for initial growth strata of  $\sim 1.4$  Ma and  $\sim 1.07$  Ma are determined from two locations along the southern flank (Figure 2). The  $\sim 1.4$  Ma age is further west and near the structural apex of the Kashi fold, and thus likely represents the initiation of fold growth. The two growth strata ages are separated by 13 km and define a lateral propagation rate of  $\sim 40$  km/ma for the Kashi Anticline [*Chen et al.*, 2007]. Thus, although both the Atushi and Kashi folds were active at 1.4 Ma, this date represents the initial growth of the Kashi Anticline whereas the Atushi Anticline likely started to deform earlier. The higher topographic expression of the Kashi Anticline, relative to the Atushi Anticline, also implies that the Kashi Anticline is younger and has eroded less than its northern counterpart.

#### 4.5.2. Shortening

[46] Shortening estimates across the Atushi and Kashi anticlines are interpreted using both surface data and seismically interpreted faults at depth. Line length reconstructions suggest between 2 and 5 km of shortening along the Atushi fold (Table 2). These estimates are similar to the line length and excess area calculations of *Scharer et al.* [2004], except at Kashi West where *Scharer et al.* [2006] estimated up to 6.8 km of shortening on the basis of surface data, whereas we interpret 3–4 km. Shortening decreases eastward along the Kashi Anticline [*Chen et al.*, 2007]. Line length estimates are based on interpreted structural geometry from the surface dips and give total shortening of 2.1 and  $\sim 0.05$  km for the Kashi West and Keketamu sections,

respectively. Minimum shortening estimates based on the excess area method are 2.6 and 0.05 km at the same sections, and also indicate an eastward decrease in shortening toward the east [*Chen et al.*, 2007].

[47] The Atushi Fault is observed in the seismic lines at all three cross sections. The fault cuts the southern flank of the Atushi fold near Kashi West section and accommodates at least 4–5 km of displacement at the surface. At depth at Kashi West, the base of the Tertiary is offset 10–12 km. By combining the 4–5 km of offset at the surface with 3–4 km across the Atushi Anticline and 2–3 km from the Kashi Anticline, shortening of the surface strata matches the shortening at depth. Similar scenarios are observed along the Keketamu and Seven Mills sections, where the correlative Atushi Fault bends along the base of the Tertiary strata and forms a fault bend fold. The Atushi Fault accommodates 7–12 km of displacement (Table 2) and is the major structure at depth. Shortening within the detachment folds in the near surface and minor backthrusting balance this faulting at depth. For example, 7–8 km of displacement across the Atushi Fault at the Keketamu section is primarily balanced by 4- to 5-km shortening at both the Atushi and Keketamu anticlines, respectively (Figure 8).

#### 4.6. Recent Shortening

[48] Although the youngest structures occur near the southern deformation front, modeling of fold-and-thrust belt evolution as critically tapered wedges suggests coeval deformation within the hinterland [e.g., *Davis et al.*, 1983]. To better constrain recent shortening at different locations within the Kashi foreland, deformed fluvial terraces in both the medial and southern foreland were surveyed with a Trimble 4700 differential GPS system. We assume that the original terrace gradient approximated the modern channel gradient, and therefore, we subtract the modern river elevation from the terrace elevation along our profile to define recent deformation.

[49] In the medial foreland, terraces are progressively tilted north along the northern flank of the Tashipishake Anticline and broad folding of the terrace surface occurs across the Middle Kashi Basin Thrust (Figure 11). The shortening produced by terrace folding, inferred from line length calculation, is less than one meter and suggests modest shortening in recent times.

[50] Deformed terraces across the Kashi and Atushi anticlines provide insight into the recent structural evolution of the southern foreland. Terraces surveyed by *Scharer et al.* [2006] show progressive tilting along the anticlinal flanks near the fold cores. These geometries have been interpreted as evidence for hinge rotation near the cores, but hinge migration toward the outer edges of the fold [*Scharer et al.*, 2006]. The survey of the Atushi Anticline presented here (Figure 13) was collected 7 km west of the Boguzihe water gap survey conducted by *Scharer et al.* [2006]. Our survey reveals recent deformation that is consistent with the kinematics of a detachment fold. Steep limbs separate a broad, gently tilted core of the fold. Crestal grabens formed near the fold apex (Figure 13b). Line length calculations along the highest terrace indicate 11 m of shortening across the

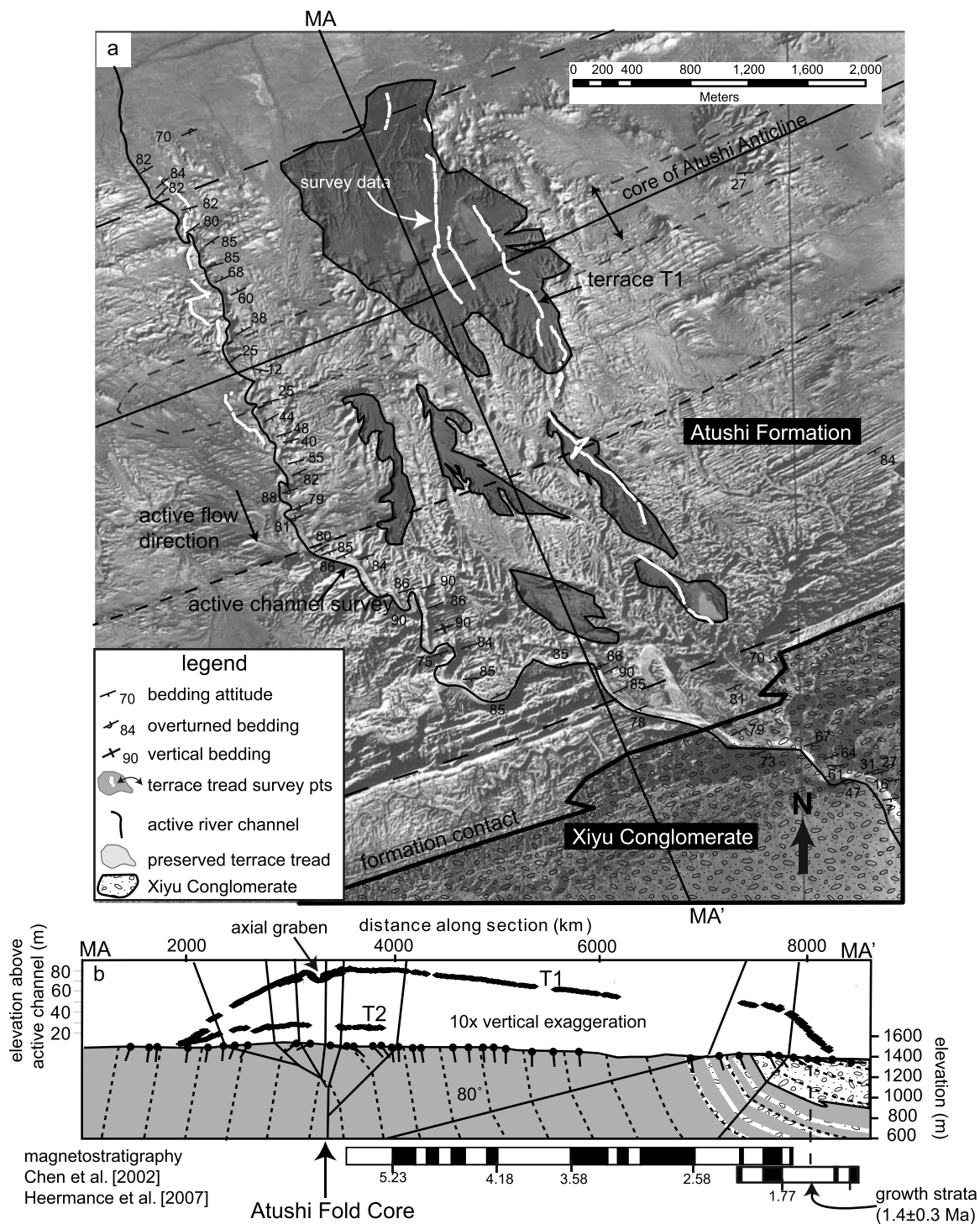


**Figure 13.** (a) Air photo and (b) structural cross section of the Middle Atushi section across the Atushi Anticline shown in Figure 6. Survey data from deformed terraces are projected perpendicular to the cross-section line, and the river gradient was removed. The terraces are shown Figure 13b with 10× vertical exaggeration and reveal the structural deformation above the Atushi Anticline. Magnetostratigraphy was correlated along bedding from ~5 km east where the section was measured along the Keketamu Anticline. Black (normal) and white (reversed) magnetozones constrain the ages of strata (shown in Ma below the magnetostratigraphy) along the southern flank of the Atushi Anticline.

8-km-long terrace. Similar broad terrace levels from the Kuqa Basin ~1000 km east have been dated at 12.5 ka [Hubert-Ferrari *et al.*, 2005]. Using 12.5 ka as an estimated age for the terrace, shortening of ~1 mm/a is calculated for the Atushi Anticline. This shortening, however, does not span the entire structural width of the fold: steeply dipping fold limbs extend north of our measured terrace (Figure 13b). Whereas more shortening could be occurring above the northern limb, the paucity of evidence for active deformation across this part of the fold suggests that the kinematics of the fold may change over time. Overall, the terrace surveys provide unambiguous evidence that ongoing deformation occurs in both the medial and southern regions of the foreland, but that deformation rates are much higher in the southern foreland.

#### 4.7. Summary of Shortening

[51] Overall, the geometry of the fold-and-thrust belt can be broadly described as a “wedge thrust” triangle zone, [Banks and Warburton, 1986; Chen *et al.*, 2004; Couzens and Wiltschko, 1996; Jones, 1996], where back thrusts and detachment folds form in front of foreland migrating fault bend folds and duplex structures. Paleozoic strata from the Tian Shan are thrust over 5–10 km of syntectonic foreland basin sedimentary strata as deformation encroaches on the foreland from the north. The result is that the hinterland region has been uplifted with respect to the foreland such that the base of the Tertiary strata is observed at the surface in the north but is buried to 5- to 10-km depth in the south.

[52] Balanced cross sections constructed from field mapping and seismic data allow us to constrain shortening at three sections across the Kashi Basin (Table 2). Total shortening within the northern foreland (Kashi Basin Thrust plus footwall imbricate structures) totals 3–9 km at Keketamu and 6–14 km at Kashi West. Shortening across the medial basin (Tashipishake, Keketamu and other associated folds and major back thrust), ranges from 6 to 10 km. Within the southern basin, surface derived shortening of 9–12 km at Kashi West, 4–5 km at Keketamu, and 2–4 km at Seven Mills is accommodated on the Keketamu, Atushi, and Kashi anticlines combined. Surface shortening determinations are approximately balanced by seismically interpreted offsets of Paleozoic strata at depth. Overall, total shortening decreases from west to east from 20 to 32 km at Kashi West, to 13–22 km at Keketamu, and to 10–19 km at Seven Mills.

## 5. Discussion

### 5.1. Timing of Deformation and Regional Implications

[53] For most ancient fold-and-thrust belts, the timing, rates, and sequence of deformation remain unknown. Even for many modern collisional belts, rarely are the age and rates of deformation well determined for each major structure. Here, in the Kashi foreland, independent age controls on deformation from at least five individual structures, combined with detailed description of their geometry and spatial relationships, allow us reconstruct the structural disruption of Kashi foreland since 25 Ma. Such thorough

age control is unique for a localized (60-km perpendicular to strike) setting and allows interpretation of how specific structures interact to affect sedimentation and structural style over time. Kashi foreland evolution can be described in four stages: Stage 1: rock uplift and shortening within the hinterland beginning at 20–25 Ma; Stage 2: displacement along the Kashi Basin Thrust and development of imbricate thrust faults in the northern foreland basin after 16.3 Ma; Stage 3: shortening across the medial basin, including growth of the Tashipishake Anticline, and associated back-thrusting or detachment folding south of the anticline from 13.5 to 4 Ma; and Stage 4: deformation of the Keketamu Anticline in the medial foreland and the Atushi and Kashi anticlines within the southern foreland after 4 Ma. Each stage is defined by its initiation but may have overlapped temporally with the other stages as deformation continued, possibly at reduced rates or out-of-sequence, during southward migration of the deformation front.

#### 5.1.1. Stage 1: Hinterland Shortening

[54] The only constraints on the initiation of hinterland deformation are 20–25 Ma apatite fission track cooling ages in the hanging wall of the South Tian Shan (STSF) and Muziduke faults [Sobel *et al.*, 2006] (Figure 2). These ages are similar to the suggested initiation of uplift for the southern Tian Shan at the Kepintage fold-and-thrust belt [Allen *et al.*, 1999; Yin *et al.*, 1998] and the Kuqa Basin [Avouac *et al.*, 1993; Sobel and Dumitru, 1997] to the east. Unlike the Kepintage thrust belt, however, Tertiary sedimentary rocks that could provide evidence of this uplift event are not exposed within the Kashi hinterland. Sedimentary evidence for 25–20 Ma uplift may be provided by detrital apatite grains within the Wuqia Group sediments >25 km south of the STSF near Wenguri village (Figure 6). These detrital grains have 25–13 Ma cooling ages [Sobel and Dumitru, 1997] that become younger up-section and were deposited in 18 to 10 Ma strata [Heermance *et al.*, 2007]. This implies that no resetting of the apatite ages occurred because of burial, and that the cooling ages represent the geothermal history of the source rocks. Whether these grains were derived from the hinterland or another source farther west, however, is uncertain. If we assume that these Miocene Wuqia Group sediments contain reset AFT grains derived from the Kashi hinterland, it follows that more than 3.5 km of exhumation on the hinterland structures, (particularly the South Tian Shan Fault) must have occurred after 25 Ma and prior to 19 Ma [Sobel *et al.*, 2006].

#### 5.1.2. Stage 2: Kashi Basin Thrust and Northern Foreland Imbricates

[55] Deformation moved south to the Kashi Basin Thrust (KBT) at  $16.3 \pm 0.3$  Ma, constrained by three observations: initial deposition of megabreccia facies, reset apatite fission track cooling ages from the hanging wall, and a three- to eight-fold acceleration in rates of sediment accumulation at two sites within the footwall. This timing correlates with findings from the Kuqa Basin ~1000 km east along the southern Tian Shan mountain front, where sedimentation rates increased at 16–17 Ma and are interpreted as the result of rapid exhumation and increased tectonic subsidence

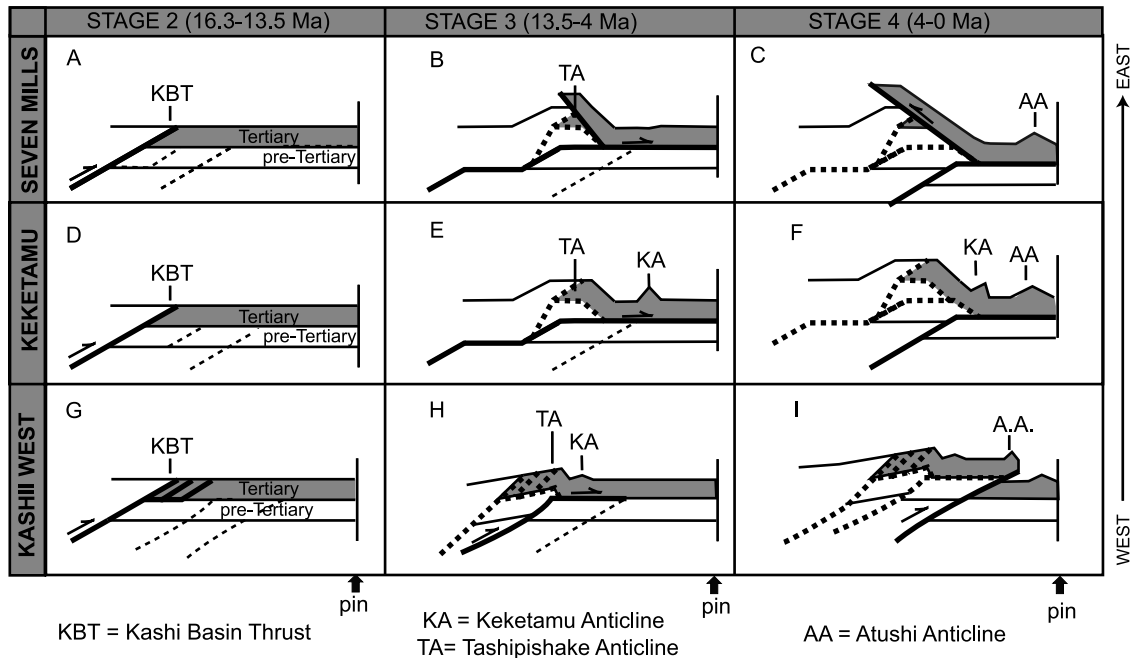


**Figure 14.** Block diagram showing the schematic structural evolution at each cross section across the Kashi Basin at stage 2 (a, d, g), stage 3 (b, e, h), and stage 4 (c, f, i). Syntectonic deposition and erosion are not shown. New structures that initiate in a given stage are labeled. Thick black lines indicate active faults, thin dotted lines are future faults, and thick dotted lines are inactive or older faults.

[Huang *et al.*, 2006]. In the Kashi foreland, this stage represents a southward shift of 15–20 km of the deformation front from the hinterland structures. The continuous trace of the KBT and similar thickness and inferred age of the footwall strata across the entire west-east width of the basin suggests that the entire length of the fault has a similar history. Differential uplift above the KBT continued for at least 1 million years after initiation, on the basis of the 0.4 mm/a sedimentation rate observed at the footwall and the more than 400 m of Xiyu Conglomerate derived from a local, high-relief source (Figure 3a). Deformation migrated south after deposition of these syntectonic strata, and displacement along footwall imbricates caused rotation of the KBT above a fault ramp. The duration of imbricate faulting is unconstrained, but the imbricate faults were subsequently rotated within the hanging wall of the Tashipishake Anticline and the imbricate faults do not deform sediments older than about 14 Ma. Thus stage 2 started with slip on the KBT and syntectonic deposition in its footwall, followed later by imbricate faulting near the base of the Tertiary strata as the deformation front migrated farther south (Figures 14a, 14d, and 14g). This stage may have been mostly terminated by ~14 Ma on the basis of the absence of strata younger than 14 Ma that are cut by these structures.

### 5.1.3. Stage 3: Medial Basin Deformation

[56] Stage 3 represents a southward migration of deformation from the Kashi Basin Thrust through the medial foreland. An increase in sedimentation rate at  $13.5 \pm 0.1$  Ma (Figure 3a) marks the initiation of growth on the Tashipishake Anticline. The development of this fault bend fold and translation of this fold above a footwall flat produced a

thrust wedge [e.g., Price, 1986] of Paleozoic strata below the weaker Tertiary units. As shortening increased, the fault bend fold slid along the footwall flat and displacement across the Paleozoic ramp must have been balanced by shortening within the Tertiary cover rocks, accommodated via back thrusting (Figure 14b) and/or detachment folding in front of the wedge (Figures 14e and 14h). Continued displacement and translation of the tectonic wedge above the footwall flat caused new structures to develop south of the deformation front over time. Localized faulting and short fold wavelengths (<1 km) imply that southward migration of deformation, though fundamentally controlled by the detachment levels within Wuqia Group strata at depth, may not have developed synchronously. A continuous, 4-km-thick stratigraphic sequence spanning from ~16–2.5 Ma was deposited in the medial foreland along the Keketamu section, and growth strata do not appear at the Keketamu Anticline within the medial foreland until ~4.0 Ma (Figure 12b). Thus, deformation must have been confined to the north of this location between 13.5 and 4 Ma: this time span defines stage 3.

### 5.1.4. Stage 4: Keketamu, Atushi, and Kashi Anticlines

[57] The ultimate stage of evolution for the Kashi foreland encompasses growth of the Keketamu, Atushi and Kashi anticlines since ~4 Ma. Direct age control of deformation is derived from five growth strata locations along the folds, and changes in sediment accumulation rates observed in the Keketamu and Atushi stratigraphic sections (Figures 2 and 3b). Our best evidence for the initiation of slip is based on 3.9–4.0 Ma growth strata at the Keketamu section (Figure 12). After this time, slip progressed south onto the

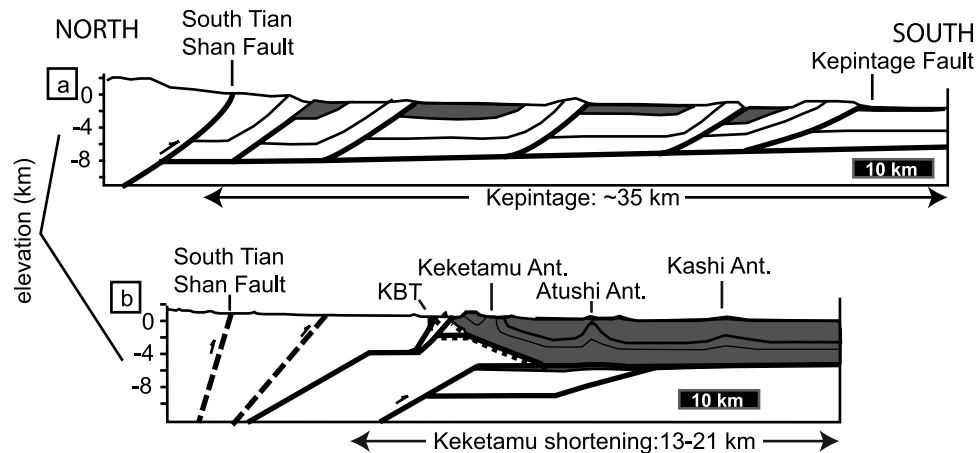


**Figure 15.** Schematic comparison between the Kepintage fold-and-thrust belt (a) and the Kashi foreland (b) structures. Tertiary strata are shown in dark gray shaded regions.

Atushi Fault at depth and coincided with continued growth of the Keketamu Anticline and back thrust displacement at Seven Mills. The Atushi and Kashi anticlines initiated by  $\sim 1.4$  Ma, likely due to continued displacement on the Atushi Fault at depth.

## 5.2. Controls on Structural Style Changes

[58] The well-constrained sequence of deformation assembled here, combined with our thorough knowledge of syntectonic strata age and thickness, allow us to evaluate changes in structural style in the context of evolving foreland stratigraphy. Prior to 25 Ma (and hence Tertiary deformation), a regional erosion surface dominated the landscape [Abdrakhmatov *et al.*, 2001; Burbank *et al.*, 1999] and is preserved as the sharp disconformity or angular unconformity that we use as a datum to measure the accumulation of syntectonic strata (Figure 4c). Changes in structural style are interpreted in the context of stratigraphic properties and thickness above this unconformity.

[59] The South Tian Shan Fault (STSF), Muziduke Fault, and Kashi Basin Thrust (KBT) all slice through the entire Paleozoic succession. These faults initiated between 25 and 16 Ma, when syntectonic strata were thinnest ( $< 3$  km). The presence of a prominent angular unconformity between the Paleozoic and overlying sedimentary units (Cretaceous or Tertiary) at all outcrops west of the Seven Mills section suggests that the Paleozoic rocks here were strongly deformed prior to the Indo-Asian collision and were not well layered when Tertiary deformation began. This deformation stands in stark contrast to the well-bedded Paleozoic strata further east in the Kepintage thrust belt [Allen *et al.*, 1999; Carroll *et al.*, 1995]. Faulting in the Kashi hinterland is dominated by planar footwall ramps that cut the upper crust. Footwall flats only occur in the near-surface where the Cretaceous and Tertiary strata are subparallel, as is seen almost ubiquitously throughout the Kashi foreland. These well-bedded, subhorizontal strata act as favorable levels for footwall detachments, as is observed within the proximal

footwall of the KBT, where the Cretaceous sandstone and shale act as the detachment levels.

[60] After  $\sim 13.5$  Ma, the structural style changed throughout the foreland to a ramp-flat, fault bend and detachment fold geometry. Although thick-skinned faults still cut through the Paleozoic strata, such as along the Atushi Fault in the Kashi West section (Figure 9) where it displaces the basal Tertiary unconformity, faults generally become subparallel to bedding and fault bend folds or detachment folds develop. In addition, this time period coincides with relatively rapid sedimentation rates  $\geq 0.4$  mm/a, causing rapid accumulation of well-bedded, syntectonic sediments within the foreland. Factors observed to influence the change in structural style include (1) the presence of well-bedded, fluvial sandstone and shale in the Pakabulake Formation between  $\sim 13.7$  and 5.3 Ma above gypsiferous shale in the lower Wuqia Group and (2) deposition of more than 8 km of horizontal, well-bedded strata. We speculate that deposition of well-bedded, weak, subhorizontal Miocene strata provided favorable zones for subhorizontal detachment faulting.

[61] At  $\sim 4.0$  Ma, detachment folding commenced at the Keketamu Anticline followed by detachment folding at  $\sim 1.4$  Ma on the Atushi and Kashi anticlines. By this time conditions in the upper 10 km of the basin were characterized by more competent, well-bedded lithologies above weak, gypsiferous detachment surfaces [Wallace and Homza, 2004]. Thus the newly developed deep Tertiary Basin with evaporitic strata was well suited for detachment folding, rather than the imbricate thrust faulting that initially deformed the basin margins.

[62] These observations can be compared with the Kepintage thrust belt located  $< 100$  km east of the Kashi Basin and distinguished by six, evenly spaced thrust faults that repeat a 4- to 6-km-thick sequence of well-bedded Paleozoic strata [Allen *et al.*, 1999; Yin *et al.*, 1998]. A detachment zone is inferred at 4–6 km within the Upper Cambrian strata, and Tertiary deposits are not more than two kilometers thick within the Kepintage region (Figure 15).

The lack of Tertiary deposition is likely due to the Bachu structural high within the Tarim Basin and below the Kepintage that suppressed accommodation space for Tertiary deposition [Allen *et al.*, 1999]. The well-layered strata observed within the Kepintage Paleozoic rocks present a stark contrast to the intensely deformed Paleozoic strata in the Kashi region (Figure 4). Where Paleozoic strata have structural inheritance (i.e., predeformed strata), thick-skinned thrusts are primarily observed in the Tian Shan [Bullen *et al.*, 2003; Burbank *et al.*, 1999; Ghose *et al.*, 1997], and flat detachments do not occur except at the stratigraphically highest levels in the Cretaceous and Tertiary lithologies. Even along strike within the Kashi Basin itself, the deep fault ramps that dominate the structural style at the western end of the foreland change to a ramp-flat style in the east at Seven Mills (Figure 7), nearer the Kepintage region. We speculate that this change is due to less deformed Paleozoic strata at Seven Mills than at Kashi West. Sub-horizontal Paleozoic strata are inferred from the seismic lines at the two eastern sections, but not at Kashi West, consistent with our hypothesis of more structural inheritance in the western Kashi Basin.

### 5.3. Deformation Rates and Comparison With GPS

[63] Shortening estimates combined with initiation ages on specific structures allow us to determine shortening rates across the Kashi foreland. Total measured shortening ranges between 11 and 32 km and spans the entire foreland (Table 2). This range encompasses estimates across all the sections but does not include shortening across the hinterland (South Tian Shan and Muziduke faults). Using an initiation age of 16.3 Ma for slip on the Kashi Basin Thrust, we calculate an average shortening rate of 0.7–1.9 mm/a, similar to the range of 1–1.9 mm/a from Yin *et al.* [1998] or the ~1.8 mm/a from Allen *et al.* [1999] calculated for the Kepintage thrust belt. Because shortening increases toward the west, shortening rates increase as well. 10–19 km of shortening over 16.3 Ma at the Seven Mills section translates to a long-term average shortening rate of 0.7–1.1 mm/a. In contrast, shortening rates at the Kashi West section based on 20- to 32-km total shortening are 1.2–1.9 mm/a. Interestingly, the increased shortening rate toward the west may be the result of clockwise rotation of the Tarim plate relative to Eurasia. Estimated present-day rotation rates are ~0.7°/Myr about an Euler pole at ~94°E, ~37°N based on geodetic measurements [Reigber *et al.*, 2001; Thatcher, 2007], or 0.45°/Myr about a pole at 96°E, 43.5°N based on differential shortening along the entire range [Avouac *et al.*, 1993]. The location of the Kashi West section ~55 km farther west from Seven Mills would account for 0.23–0.65 mm/a increased shortening, or approximately the difference between the observed rates for each section. The shortening rates presented here are long-term averages calculated over millions of years, and thus it is difficult to reconcile these rates with short-term geodetic rates averaged over only a few years. Furthermore, our observed shortening gradient could be simply the result of local rotation [Dupont-Nivet *et al.*, 2002] or due to impingement of the Pamir asymmetrically on the western Tarim Basin. Never-

theless the observed similarity between our long-term averages with geodetic rates are remarkable, and suggest that changes in shortening along strike within the Kashi foreland may be the result of clockwise rotation of the Tarim relative to Eurasia.

[64] Our age constraints and detailed study of individual structures allow us to further dissect the deformation rates at specific time periods (Figure 16). The most recent deformation occurs during Stage 4 along the Keketamu, Atushi, and Kashi anticlines since ~4 Ma. Growth strata and sedimentation rate changes are inferred from strata near the Keketamu section, and therefore we focus on this section for our analysis. 8–10 km of shortening across the Keketamu and Atushi anticlines at the Keketamu cross section (Figure 8) since 4 Ma accounts for 2.25–2.75 mm/a of shortening (Figure 16). The range in rate is due to the uncertainty in shortening magnitude and age of the shortening event. In contrast, shortening rates of <0.5 mm/a occurred during stage 3 within the medial basin, on the basis of only 2- to 3-km shortening between 13.5 and 4 Ma across the Tashipishake Anticline. Stage 2 shortening of 3–9 km across the Kashi Basin Thrust and associated imbricate faults occurred between 16.3 and 13.5 Ma at a rate of 1.1–3.2 mm/a. Prior to ~16.3 Ma, the total shortening is unconstrained. Nevertheless, these data suggest that shortening rates circa 16 Ma were 1.1–3.2 mm/a, decreased by at least 50% from 13 to 4 Ma, and increased at least fourfold after 4 Ma (Figure 16). Similar, several-fold increases in deformation rates have been interpreted for the Kyrgyz Tian Shan at 11 Ma and 3 Ma [Bullen *et al.*, 2001], for the Kashi foreland on the basis of thermochronology [Sobel *et al.*, 2006], and for both the northern and southern Tian Shan foreland 1000 km east of the study since 0.2–0.3 Ma [Daeron *et al.*, 2007; Hubert-Ferrari *et al.*, 2005].

[65] Our data suggest that, even across a fairly broad foreland deformation belt as found in the Kashi foreland, shortening rates can display strong temporal variation. For the Tian Shan with its many ranges encompassed between the Tarim Basin and the Kazakh platform, the episodic rates described above suggest that the locus of deformation shifted in and out of the foreland and was accommodated at a broad suite of sites within the larger range. Despite rates up to 3 mm/a calculated during stages 2 and 4, shortening rates remain considerably less than the 7–8 mm/a expected from GPS data [Abdrakhmatov *et al.*, 1996; Reigber *et al.*, 2001].

[66] Palinspastic reconstruction (Figure 17) of the Keketamu section combined with precise age control on many of the structures therein permits the calculation of the southward propagation rate of deformation into the basin. Between 25 and 16.3 Ma during stage 1, only the South Tian Shan and Muziduke faults were active. However, these faults are located today some 29 and 18 km north of the Kashi Basin Thrust, respectively, and were likely >8–10 km farther north prior to the (poorly defined) shortening across them. Thus, the deformation front migrated more than 29 km over 3.7–8.7 million years (assuming initiation of shortening at 20–25 Ma), yielding a propagation rate of 3.3–7.7 mm/a (Figure 16c). As imbricate thrusts formed in the

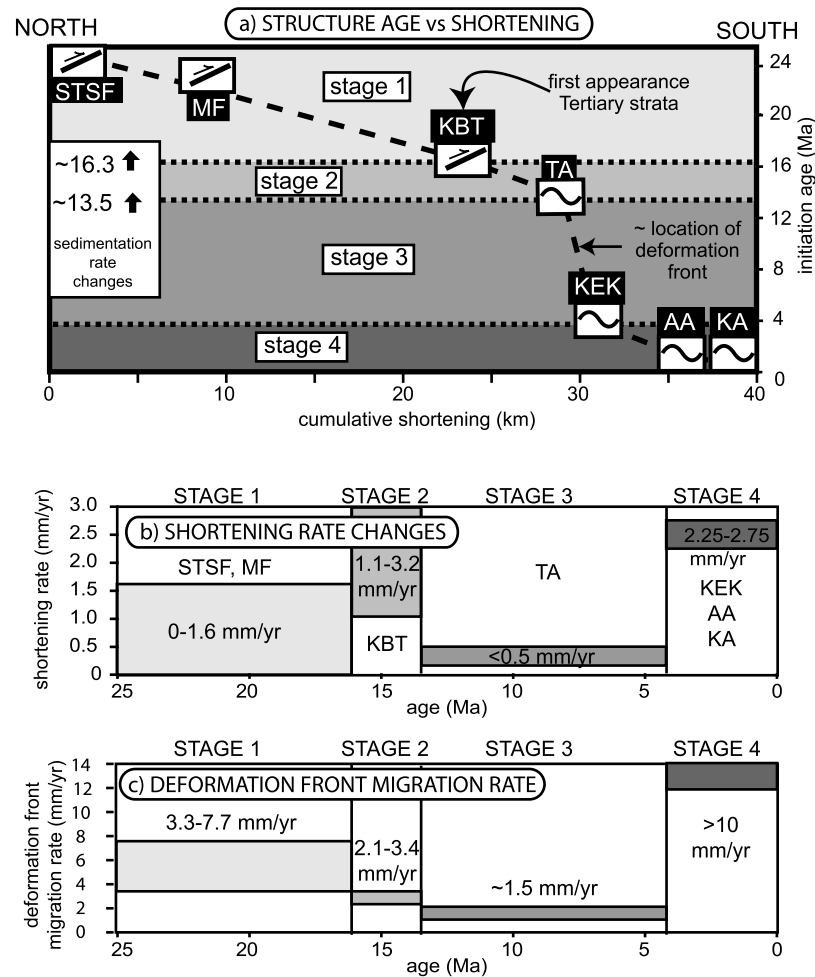


**Figure 16.** Determination of differential shortening and structural migration rates. (a) Plot of cumulative shortening within the Kashi foreland against the initiation age of each structure. STSF, South Tian Shan Fault; MF, Muziduke Fault; KBT, Kashi Basin Thrust; TA, Tashipishake Anticline; KEK, Keketamu Anticline; AA, Atushi Anticline; KA, Kashi Anticline. (b) Plot of the variable shortening rates (shown as shaded zones) during the different deformation stages. (c) Plot showing the different rates (shaded zones) that the deformation front migrates southward within the Kashi foreland over time.

KBT footwall, propagation rates into the basin slowed to 2.1–3.4 mm/a between 16.3 and 13.5 Ma. Another deceleration to <1.5 mm/a occurred between 13.5 and 4 Ma, prior to accelerating to more than 10 mm/a after 4 Ma.

[67] Causes for such changes in propagation rates are likely linked to changing shortening rates: one would expect that slower shortening rates would likewise decrease propagation rates (Figure 16). We speculate that major changes in structural style modulated propagation rates. The switch from deep-seated thrusting to detachment folding facilitated rapid propagation of the deformation front. When deep-seated thrusts dominate, the deformation front migrates only when new faults rupture up through the strongly deformed Paleozoic succession. Commonly, slip on an existing fault is energetically advantageous compared to forming a new one [Hilley *et al.*, 2005], such that creation of new faults is infrequent, new faults are most likely to form quite close to

existing faults, and propagation rates are slow. In contrast, when weak zones exist within a well-bedded sedimentary sequence, deeper slip on thick-skinned thrusts can transfer on to gently dipping detachment surfaces and rapidly propagate into a foreland. Hence, we speculate that the thick Kashi foreland strata with its weak evaporitic layers promoted very rapid propagation of the deformation front over the past 2 million years.

[68] Our detailed chronology of deformation within the Kashi foreland documents the high variability in shortening rates during the outward migration of deformation. In addition, deformed terraces from across the foreland suggest that modern deformation rates are much higher along the southern edge of the deformation front. Slow deformation continues, however, in the hinterland, where growth strata within the PBB and deformed terraces suggest slow but continuing deformation. Such continued hinterland shorten-

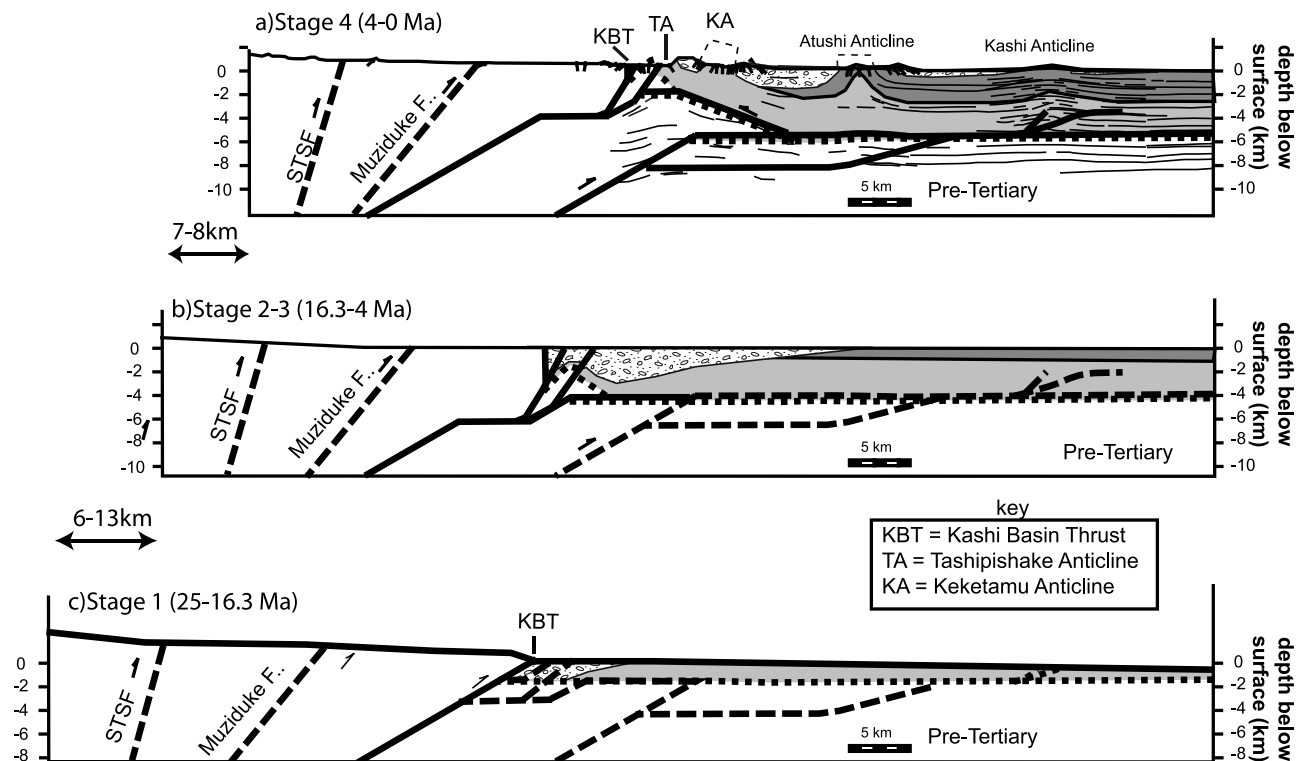


**Figure 17.** Palinspastic reconstruction of the Keketamu section at stages 4 (a), 2–3 (b), and 1 (c). Faults are the thick black lines, dashed where inferred. The dotted line indicates the base of the Tertiary strata.

ing is expected as the orogenic wedge adjusts in order to maintain a critical taper in the context of rapid sedimentation in front of the range and ongoing erosion within it [Dahlen, 1990; Storti and McClay, 1995]. This distributed shortening highlights the complexity of deformation within an active foreland.

## 6. Conclusions

[69] The Kashi foreland contains a well-dated Neogene stratigraphy that provides a foundation for understanding the structural and stratigraphic evolution of the region over time. Seven major structures have been mapped and their initiation ages determined by a combination of hanging wall cooling ages [Sobel *et al.*, 2006], sediment accumulation rate changes, crosscutting relationships, and growth strata ages. This is now one of the best-dated foreland successions in the world. Deformation has migrated south more than 40 km since the latest Oligocene in four stages. The initial stages result from slip on thick-skinned faults that slice through the upper crust, whereas later stages involve fault bend folding at depth and detachment folding near the surface.

[70] On the basis of our three balanced sections, shortening decreases from west to east across the foreland and is consistent with the gradient predicted by the clockwise rotation of the Tarim block with respect to the Tian Shan. During the past 16 million years, shortening has been strikingly unsteady within the Kashi foreland. The thrust

front has propagated southward into the foreland episodically and at irregular rates. Concurrently, rates of shortening have accelerated and decelerated several times. The most rapid migration of the deformation front occurred during the Plio-Pleistocene and seems to have resulted from the onset of widespread detachment folding above extensive weak strata within the Tertiary foreland succession. Whereas present-day deformation is most active along the southern margin of the fold-and-thrust belt where deformation initiated most recently, the hinterland continues to deform, albeit at a much slower rate than the deformation front.

[71] In the Kashi foreland, changes in structural styles correlate with changes in Paleozoic-to-Tertiary stratigraphy. Detachment folds are ubiquitous along the southern deformation front, whereas toward the hinterland, fault bend and fault propagation folds become the norm. Structural style varies because of (1) the presence of inherited structures within the Paleozoic strata [Allen *et al.*, 1991], (2) the development of new, thick-skinned thrust faults that rupture through the strongly deformed Paleozoic strata, and (3) both the thickness of the syntectonic Tertiary strata and the distribution of weak evaporitic layers within them. Thrust flats are most likely to form where coherent layers of weak strata are present within the footwall. In the Kashi foreland, where the Paleozoic footwall rocks were previously deformed such that subhorizontal planes of weakness are uncommon, fault ramps propagate through the deformed rocks to the surface. When a ramp intercepts subhorizontal, well-bedded, weak strata such as the Wuqia Group gypsif-

erous shales, the fault bends to exploit the weak bedding and forms a new detachment horizon. Deposition of weak shale horizons within the active foreland provided favorable detachment planes for the thrust flats and thus wedge thrusts and detachment folding become the dominant structural style.

[72] **Acknowledgments.** We thank Eric Kirby, Ramon Gonzalez-Mieres, and an anonymous reviewer for their thoughtful reviews. We are grateful to PetroChina for permission to use the seismic lines presented in this manuscript. Fieldwork assistance and discussion with Feng Wunquan, Kate Schärer, Patricia Ruano, and Changsheng Wang was much appreciated. This research was supported by U.S. National Science Foundation grant EAR-0230403, National Science Foundation of China grants 40372081 and 40672109.

## References

- Abdrakhmatov, K. Y., et al. (1996), Relatively recent construction of the Tien/Shan inferred from GPS measurements of present-day crustal deformation rates, *Nature*, *384*, 450–453.
- Abdrakhmatov, K., et al. (2001), Onset, style and current rate of shortening in the central Tien Shan, Kyrgyz Republic, *Russ. Geol. Geophys.*, *42*, 1585–1609.
- Allen, M. B., et al. (1991), Basin evolution within and adjacent to the Tien Shan range, NW China, *J. Geol. Soc.*, *148*, 369–378, doi:10.1144/gsjgs.148.2.0369.
- Allen, M. B., B. F. Windley, and Z. Chi (1999), Late Cenozoic tectonics of the Kepingtage thrust zone: Interactions of the Tien Shan and Tarim Basin, northwest China, *Tectonics*, *18*, 639–654, doi:10.1029/1999TC900019.
- Amos, C. D., D. W. Burbank, D. C. Nobes, and S. A. L. Read (2007), Geomorphic constraints on listric thrust faulting: Implications for active deformation in the Mackenzie Basin, South Island, New Zealand, *J. Geophys. Res.*, *112*, B03S11, doi:10.1029/2006JB004291.
- Armstrong, F. C., and S. S. Oriol (1965), Tectonic development of Idaho-Wyoming thrust belt, *AAPG Bull.*, *49*, 1847–1866.
- Avouac, J.-P., P. Tapponnier, M. Bai, H. You, and G. Wang (1993), Active thrusting and folding along the northern Tien Shan and late Cenozoic rotation of the Tarim relative to Dzungaria and Kazakhstan, *J. Geophys. Res.*, *98*, 6755–6804, doi:10.1029/92JB01963.
- Bally, A. W., et al. (1986), Notes on sedimentary basins in China, *U.S. Geol. Surv. Open File Rep.*, *86-327*, 108 pp.
- Banks, C. J., and J. Warburton (1986), “Passive-roof” duplex geometry in the frontal structures of the Kirthar and Sulaiman mountain belts, Pakistan, *J. Struct. Geol.*, *8*, 229–237, doi:10.1016/0191-8141(86)90045-3.
- Blair, T. C., and J. G. McPherson (1999), Grain-size and textural classification of coarse sedimentary particles, *J. Sediment. Res.*, *69*, 6–19.
- Boyer, S. E. (1992), Geometric evidence for synchronous thrusting in the southern Alberta and northwest Montana thrust belts, in *Thrust Tectonics*, edited by K. R. McClay, pp. 377–390, Chapman and Hall, Suffolk, UK.
- Bullen, M. E., D. W. Burbank, K. Y. Abdrakhmatov, and J. Garver (2001), Late Cenozoic tectonic evolution of the northwestern Tien Shan: Constraints from magnetostratigraphy, detrital fission track, and basin analysis, *Geol. Soc. Am. Bull.*, *113*, 1544–1559, doi:10.1130/0016-7606(2001)113<1544:LCTEOT>2.0.CO;2.
- Bullen, M. E., D. W. Burbank, and J. Garver (2003), Building the northern Tien Shan: Integrated thermal, structural, and topographic constraints, *J. Geol.*, *111*, 149–165, doi:10.1086/345840.
- Burbank, D. W., and R. G. H. Raynolds (1984), Sequential late Cenozoic structural disruption of the northern Himalayan foredeep, *Nature*, *311*, 114–118, doi:10.1038/311114a0.
- Burbank, D. W., J. K. McLean, M. Bullen, K. Y. Abdrakhmatov, and M. G. Miller (1999), Partitioning of intermontane basins by thrust-related folding, Tien Shan, Kyrgyzstan, *Basin Res.*, *11*, 75–92, doi:10.1046/j.1365-2117.1999.00086.x.
- Burchfiel, B. C., et al. (1999), Crustal shortening on the margins of the Tien Shan, Xinjiang, China, *Int. Geol. Rev.*, *41*, 665–700.
- Carroll, A. R., S. A. Graham, M. S. Hendrix, D. Ying, and D. Zhou (1995), Late Paleozoic tectonic amalgamation of northwestern China: Sedimentary record of the northern Tarim, northwestern Turpan, and southern Junggar basins, *Geol. Soc. Am. Bull.*, *107*, 571–594, doi:10.1130/0016-7606(1995)107<0571:LPTAON>2.3.CO;2.
- Charlesworth, H. A. K., and L. G. Gagnon (1985), Intercutaneous wedges, the triangle zone and structural thickening of the Mynheer coal seam at Coal Valley in the Rocky-Mountain foothills of central Alberta, *Bull. Can. Pet. Geol.*, *33*, 22–30.
- Charreau, J., et al. (2005), Magnetostratigraphy and rock magnetism of the Neogene Kuitun He section (northwest China): Implications for late Cenozoic uplift of the Tianshan Mountains, *Earth Planet. Sci. Lett.*, *230*, 177–192, doi:10.1016/j.epsl.2004.11.002.
- Charreau, J., et al. (2006), Magnetostratigraphy of the Yaha section, Tarim Basin (China): 11 Ma acceleration in erosion and uplift of the Tien Shan Mountains, *Geology*, *34*, 181–184, doi:10.1130/G22106.1.
- Chen, J., et al. (2001), Late Cenozoic tectonics and seismicity in the southwestern Tien Shan, China, *Earthquake Res. China*, *17*, 134–155.
- Chen, J., et al. (2002), Magnetostratigraphy of the Upper Cenozoic strata in the southwestern Chinese Tien Shan: Rates of Pleistocene folding and thrusting, *Earth Planet. Sci. Lett.*, *195*, 113–130, doi:10.1016/S0012-821X(01)00579-9.
- Chen, J., et al. (2007), Quantification of growth and lateral propagation of the Kashi Anticline, Southwestern Chinese Tien Shan, *J. Geophys. Res.*, *112*, B03S16, doi:10.1029/2006JB004345.
- Chen, S., L. Tang, Z. Jin, C. Jia, and X. Pi (2004), Thrust and fold tectonics and the role of evaporites in deformation in the western Kuqa foreland of Tarim Basin, northwest China, *Mar. Pet. Geol.*, *21*, 1027–1042, doi:10.1016/j.marpetgeo.2004.01.008.
- Clift, P. (2006), Controls on the erosion of Cenozoic Asia and the flux of clastic sediment of the ocean, *Earth Planet. Sci. Lett.*, *241*, 571–580, doi:10.1016/j.epsl.2005.11.028.
- Couzens, B. A., and D. V. Wiltshko (1996), The control of mechanical stratigraphy on the formation of triangle zones, *Bull. Can. Pet. Geol.*, *44*, 165–179.
- Crowley, P. D., P. W. Reiners, J. M. Reuter, and G. D. Kaye (2002), Laramide exhumation of the Bighorn Mountains, Wyoming: An apatite (U-Th)/He thermochronology study, *Geology*, *30*, 27–30, doi:10.1130/0091-7613(2002)030<0027:LEOTBM>2.0.CO;2.
- Daeron, M., J. Avouac, and J. Charreau (2007), Modeling the shortening history of a fault-tip fold using structural and geomorphic records of deformation, *J. Geophys. Res.*, *112*, B03S13, doi:10.1029/2006JB004460.
- Dahlen, F. A. (1990), Critical taper model of fold-and-thrust belts and accretionary wedges, *Annu. Rev. Earth Planet. Sci.*, *18*, 55–99, doi:10.1146/annurev.ea.18.050190.000415.
- Dahlen, F. A., J. Suppe, and D. Davis (1984), Mechanics of fold-and-thrust belts and accretionary wedges: Cohesive Coulomb theory, *J. Geophys. Res.*, *89*, 10,087–10,101.
- Dahlstrom, C. D. A. (1970), Structural geology of the eastern margin of the Canadian Rocky Mountains, *Bull. Can. Pet. Geol.*, *18*, 332–406.
- Davis, D., J. Suppe, and F. A. Dahlen (1983), Mechanics of fold-and-thrust belts and accretionary wedges, *J. Geophys. Res.*, *88*, 1153–1172, doi:10.1029/JB088iB02p01153.
- Decelles, P. G., and K. A. Giles (1996), Foreland basins systems, *Basin Res.*, *8*, 105–123, doi:10.1046/j.1365-2117.1996.01491.x.
- Delcaillau, B., et al. (1998), Morphotectonic evidence from lateral propagation of an active frontal fold: Pakuashan Anticline, foothills of Taiwan, *Geomorphology*, *24*, 263–290, doi:10.1016/S0169-555X(98)00020-8.
- Dumitru, T. A., et al. (2001), Uplift, exhumation, and deformation in the Chinese Tien Shan, *Mem. Geol. Soc. Am.*, *194*, 71–99.
- Dupont-Nivet, G., Z. Guo, R. F. Butler, and C. Jia (2002), Discordant paleomagnetic direction in Miocene rocks from the central Tarim Basin: Evidence for local deformation and inclination shallowing, *Earth Planet. Sci. Lett.*, *199*, 473–482, doi:10.1016/S0012-821X(02)00566-6.
- Epard, J. L., and R. H. Goshong Jr. (1993), Excess area and depth to detachment, *Am. Assoc. Pet. Geol. Bull.*, *77*, 1291–1302.
- Ghose, S., R. J. Mellors, A. M. Korjenkov, M. W. Hamburger, T. L. Pavlis, G. L. Pavlis, M. Omuraliev, E. Mamyrov, and A. R. Muraliev (1997), The MS = 7.3 1992 Suusamy, Kyrgyzstan, earthquake in the Tien Shan: 2. Aftershock focal mechanisms and surface deformation, *Bull. Seismol. Soc. Am.*, *87*(1), 23–38.
- Gonzalez-Mieres, R., and J. Suppe (2006), Relief and shortening in detachment folds, *J. Struct. Geol.*, *28*, 1785–1807, doi:10.1016/j.jsg.2006.07.001.
- Guo, Z. T., W. F. Ruddiman, Q. Z. Hao, H. B. Wu, Y. S. Qiao, R. X. Zhu, S. Z. Peng, J. J. Wei, B. Y. Yuan, and T. S. Liu (2002), Onset of Asian desertification by 22 Myr ago inferred from loess deposits in China, *Nature*, *416*, 159–163, doi:10.1038/416159a.
- Heermance, R. V., J. Chen, D. W. Burbank, and C. S. Wang (2007), Tectonic control on gravel progradation and the significance of upward coarsening stratigraphy in the evolving southwestern Chinese Tien Shan foreland, *Basin Res.*, *19*, 599–632, doi:10.1111/j.1365-2117.2007.00339.x.
- Hendrix, M. S., et al. (1992), Sedimentary record and climatic implications of recurrent deformation in the Tien Shan: Evidence from Mesozoic strata of the North Tarim, South Junggar and Turpan basins, Northwest China, *Geol. Soc. Am. Bull.*, *104*, 53–79, doi:10.1130/0016-7606(1992)104<0053:SRACIO>2.3.CO;2.
- Hendrix, M. S., T. A. Dumitru, and S. A. Graham (1994), Late Oligocene-early Miocene unroofing in the Chinese Tien Shan: An early effect of the India-Asia collision, *Geology*, *22*, 487–490, doi:10.1130/0091-7613(1994)022<0487:LOEMUI>2.3.CO;2.
- Hilley, G. E., P. M. Blisniuk, and M. R. Strecker (2005), Mechanics and erosion of basement-cored uplift provinces, *J. Geophys. Res.*, *110*, B12409, doi:10.1029/2005JB003704.
- Huang, B., et al. (2006), Magnetostratigraphic study of the Kuche Depression, Tarim Basin, and Cenozoic

- uplift of the Tian Shan range, western China, *Earth Planet. Sci. Lett.*, 251, 346–364, doi:10.1016/j.epsl.2006.09.020.
- Hubert-Ferrari, A., J. Suppe, J. Van der Woerd, X. Wang, and H. F. Lu (2005), Irregular earthquake cycle along the southern Tianshan front, Aksu area, China, *J. Geophys. Res.*, 110, B06402, doi:10.1029/2003JB002603.
- Husson, L., J. L. Mugnier, P. Leturmy, and G. Vidal (2003), Kinematics and sedimentary balance of the Subhimalayan range, W. Nepal, in *Thrust Tectonics and Hydrocarbon Systems*, edited by K. McClay, pp. 1–16, Am. Assoc. of Pet. Geol., Houston, Tex.
- Ji, J., P. Luo, P. White, H. Jiang, L. Gao, and Z. Ding (2008), Episodic uplift of the Tianshan Mountains since the late Oligocene constrained by magnetostratigraphy of the Jingou River section, in the southern margin of the Junggar Basin, China, *J. Geophys. Res.*, 113, B05102, doi:10.1029/2007JB005064.
- Jia, C., S. Zhang, and S. Wu (2004), *Stratigraphy of the Tarim Basin and Adjacent Areas* (in Chinese with English abstract), 1063 pp., Sci. Press, Beijing.
- Jones, P. B. (1996), Triangle zone geometry, terminology and kinematics, *Bull. Can. Petrol. Geol.*, 44(2), 139–152.
- Jordan, T. E., R. W. Allmendinger, J. F. Damanti, and R. E. Drake (1993), Chronology of motion in a complete thrust belt: The Precordillera, 30–31°S, Andes Mountains, *J. Geol.*, 101, 135–156.
- Kao, H., and W.-P. Chen (2000), The Chi-Chi earthquake sequence: Active, out-of-sequence thrust faulting in Taiwan, *Science*, 288, 2346–2349, doi:10.1126/science.288.5475.2346.
- Lavé, J., and J. P. Avouac (2000), Active folding of fluvial terraces across the Siwalik Hills, Himalaya of central Nepal, *J. Geophys. Res.*, 105, 5735–5770, doi:10.1029/1999JB900292.
- Lourens, L. J., F. J. Hilgen, J. Laskar, N. J. Shackleton, and D. Wilson (2005), The Neogene period, in *Geological Time Scale*, edited by F. M. Gradstein et al., pp. 409–440, Cambridge Univ. Press, Cambridge, UK.
- Medwedeff, D. A. (1992), Geometry and kinematics of an active, laterally propagating wedge thrust, Wheeler Ridge, California, in *Structural Geology of Fold and Thrust Belts*, edited by S. Mitra and G. W. Fisher, pp. 3–28, Johns Hopkins Univ. Press, Baltimore, Md.
- Meigs, A. J., and D. W. Burbank (1997), Growth of the South Pyrenean orogenic wedge, *Tectonics*, 16, 239–258, doi:10.1029/96TC03641.
- Métivier, F., and Y. Gaudemer (1997), Mass transfer between eastern Tien Shan and adjacent basins (central Asia): Constraints on regional tectonics and topography, *Geophys. J. Int.*, 128, 1–17, doi:10.1111/j.1365-246X.1997.tb04068.x.
- Mitra, S. (2002), Structural models of faulted detachment folds, *Am. Assoc. Petrol. Geol. Bull.*, 86, 1673–1694.
- Molnar, P. (2004), Late Cenozoic increase in accumulation rates of terrestrial sediment: How might climate change have affected erosion rates?, *Annu. Rev. Earth Planet. Sci.*, 32, 67–89, doi:10.1146/annurev.earth.32.091003.143456.
- Molnar, P., and P. Tapponnier (1975), Cenozoic tectonics of Asia: Effects of a continental collision, *Science*, 189, 419–426, doi:10.1126/science.189.4201.419.
- Morley, C. K. (1988), Out-of-sequence thrusts, *Tectonics*, 7, 539–561, doi:10.1029/TC007i003p00539.
- Mulder, T. J., and D. W. Burbank (1993), Changes in patterns of fluvial deposition resulting from initial uplift of the Salt range, northwest Himalayan foreland, Pakistan, in *Alluvial Sedimentation*, edited by M. Marzo and C. Puigdefabregas, pp. 521–539, Blackwell Sci. Publ., Oxford, UK.
- Najman, Y., K. Johnson, N. White, and G. Oliver (2004), Evolution of the Himalayan foreland basin, NW India, *Basin Res.*, 16, 1–24, doi:10.1111/j.1365-2117.2004.00223.x.
- Poblet, J., and K. McClay (1996), Geometry and kinematics of single-layer detachment folds, *Am. Assoc. Pet. Geol. Bull.*, 80, 1085–1109.
- Price, R. A. (1986), The southeastern Canadian Cordillera: Thrust faulting, tectonic wedging, and delamination of the lithosphere, *J. Struct. Geol.*, 8, 239–254, doi:10.1016/0191-8141(86)90046-5.
- Reigber, C., et al. (2001), New space geodetic constraints on the distribution of deformation in central Asia, *Earth Planet. Sci. Lett.*, 191, 157–165, doi:10.1016/S0012-821X(01)00414-9.
- Riba, O. (1976), Syntectonic unconformities of the Alto Cardener, Spanish Pyrenees: A genetic interpretation, *Sed. Geol.*, 15, 213–233, doi:10.1016/0037-0738(76)90017-8.
- Scharer, K. M., D. W. Burbank, J. Chen, R. J. Weldon, C. Rubin, R. Zhao, and J. Shen (2004), Detachment folding in the southwestern Tian Shan: Tarim foreland, China: Shortening estimates and rates, *J. Struct. Geol.*, 26, 2119–2137, doi:10.1016/j.jsg.2004.02.016.
- Scharer, K., D. W. Burbank, J. Chen, and R. Weldon (2006), Kinematic models of fluvial terraces over active detachment fold: Constraints on the growth mechanism of the Kashi-Atushi fold system, Chinese Tian Shan, *Geol. Soc. Am. Bull.*, 118, 1006–1021, doi:10.1130/B25835.1.
- Seeber, L., J. G. Armbruster, and R. C. Quittmeyer (1981), Seismicity and continental subduction in the Himalayan arc, in *Zagros, Hindu Kush, Himalaya Geodynamic Evolution*, edited by H. K. Gupta and F. M. Delaney, pp. 215–242, AGU, Washington, D. C.
- Simoës, M., et al. (2007), Kinematic analysis of the Pakuashan Fault tip fold, west central Taiwan: Shortening rate and age of folding inception, *J. Geophys. Res.*, 112, B03S14, doi:10.1029/2005JB004198.
- Sobel, E. R., and T. Dumitru (1997), Thrusting and exhumation around the margins of the western Tarim Basin during the India-Asia collision, *J. Geophys. Res.*, 102, 5043–5064, doi:10.1029/96JB03267.
- Sobel, E., J. Chen, and R. V. Heermance (2006), Late Oligocene: Early Miocene initiation of shortening in the southwestern Chinese Tian Shan: Implications for Neogene shortening rate variations, *Earth Planet. Sci. Lett.*, 247, 70–81, doi:10.1016/j.epsl.2006.03.048.
- Storti, F., and K. McClay (1995), Influence of syntectonic sedimentation on thrust wedges in analogue models, *Geology*, 23, 999–1002, doi:10.1130/0091-7613(1995)023<0999:IOSSOT>2.3.CO;2.
- Sun, J., R. X. Zhu, and J. Bowler (2004), Timing of the Tianshan Mountains uplift constrained by magnetostratigraphic analysis of molasse deposits, *Earth Planet. Sci. Lett.*, 219, 239–253, doi:10.1016/S0012-821X(04)00008-1.
- Suppe, J. (1983), Geometry and kinematics of fault bend folding, *Am. J. Sci.*, 283, 648–721.
- Thatcher, W. (2007), Microplate model for the present-day deformation of Tibet, *J. Geophys. Res.*, 112, B01401, doi:10.1029/2005JB004244.
- Vergés, J., M. Marzo, and J. A. Muñoz (2002), Growth strata in foreland settings, *Sed. Geol.*, 146, 1–9, doi:10.1016/S0037-0738(01)00162-2.
- Wallace, W. K., and T. X. Homza (2004), Detachment folds versus fault-propagation folds, and their truncation by thrust faults, *AAPG Mem.*, 82, 324–355.
- Wang, Q., et al. (2001), Present-day crustal deformation in China constrained by global positioning system measurements, *Science*, 294, 574–577, doi:10.1126/science.1063647.
- Willett, S. D. (1999), Orogeny and orography: The effects of erosion on the structure of mountain belts, *J. Geophys. Res.*, 104, 28,957–28,982, doi:10.1029/1999JB900248.
- Windley, B. F., M. B. Allen, C. Zhang, Z.-Y. Zhao, and G.-R. Wang (1990), Paleozoic accretion and Cenozoic reformation of the Chinese Tien Shan range, central Asia, *Geology*, 18, 128–131, doi:10.1130/0091-7613(1990)018<0128:PAACRO>2.3.CO;2.
- Xinjiang Bureau of Geology and Mineral Resources (1993), *Regional Geology of the Xinjiang Uygur Autonomous Region*, 561 pp., Geol. Publ. House, Beijing.
- Yin, A., S. Nie, P. Craig, T. M. Harrison, F. J. Ryerson, X. Qian, and G. Yang (1998), Late Cenozoic tectonic evolution of the southern Chinese Tian Shan, *Tectonics*, 17, 1–17, doi:10.1029/97TC03140.
- Yin, A., et al. (2002), Tectonic history of the Altyn Tagh Fault system in northern Tibet inferred from Cenozoic sedimentation, *Geol. Soc. Am. Bull.*, 114, 1257–1295, doi:10.1130/0016-7606(2002)114<1257:THOTAT>2.0.CO;2.
- Zhang, H. N. (1989), Geochemical characteristics and resource prediction of Meso-Cenozoic source rocks in Tarim, in *Petroleum Resources: Prospects and Evaluations, Selected Papers on Petroleum and Natural Gas Geology*, edited by Inst. of Pet. Geol. of the Min. of Geol. and Min. Resour., pp. 53–76, Geol. Publ., Beijing.

D. W. Burbank, Department of Earth Science, University of California, Santa Barbara, CA 93106, USA.

J. Chen, State Key Laboratory of Earthquake Dynamics, Institute of Geology, China Earthquake Administration, Beijing 100029, China.

R. V. Heermance, U.S. Geological Survey, 520 North Park Avenue, Suite 355, Tucson, AZ 85719, USA. (rheermance@usgs.gov)

J. Miao, Research Institute of Petroleum Exploration and Development, PetroChina, Beijing 100083, China.